Boundary Element Simulation of Oscillating Foil with Leading-Edge Separation

by

Xiaoxia Dong

Submitted to the Department of Mechanical Engineering
in partial fulfillment of the requirements for the degree of

Master of Science

at the
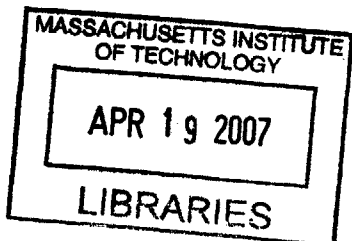
MASSACHUSETTS INSTITUTE OF TECHNOLOGY

[February 2007]

Feberary 2007

Author . . . .
Department of Mechanical Engineering
January 25, 2007

Certified by . . . .
Dick K. P. Yue
Professor of Mechanical and Ocean Engineering
Thesis Supervisor

Accepted by . . . .
Lallit Anand
Professor of Mechanical Engineering
Chairman, Department Committee on Graduate Students

Boundary Element Simulation of Oscillating Foil with Leading-Edge Separation

by

Xiaoxia Dong

Abstract

In this thesis, we develop a numerical model to account for the leading-edge separation for the boundary element simulation of the oscillating foil with potential flow assumption.

Similar to the trailing-edge separation, the leading-edge separation is modeled by a thin shear layer. Because the leading edge is rounded which is different from the sharp trailing edge, the location for leading-edge separation is extremely difficult to predetermine especially when the flow is unsteady. For unsteady flows, the position of the leading-edge separation may vary with time. However, we present a criterion that is related to the adverse pressure gradient to predict the location for the leading-edge separation. Because of the Lagrange scheme of the wake relaxation in the boundary element simulation, the leading-edge wake sheet goes into or through the thin foil easily. In order to solve the problem of the wake penetration into the foil, we present an algorithm to deal with the penetration of the leading-edge wake into the foil body.

We simulate the oscillating foil in heaving-pitching motions with our leading-edge model by the boundary element method to compare with the experiments. Without accounting for leading-edge separation, the predictions of the thrust coefficient and the propulsion efficiency of a heaving-pitching foil are good only when the Strouhal number or the maximum angle of attack is small. With our model of the leading-edge separation, the predictions are improved significantly at a larger range of Strouhal numbers or maximum angles of attack because leading-edge separation becomes significant at large Strouhal numbers or maximum angles of attack. Further possible improvements of this leading-edge separation model are discussed.

Thesis Supervisor: Dick K. P. Yue
Title: Professor of Mechanical and Ocean Engineering

2

Acknowledgments

First I would like to thank my thesis advisor, Professor Dick K.P.Yue, for his support academically and financially. His sharp advices are very benefitial not only in research, but also in the way of how to do research and how to present our research work. His comments on research notes are very impressive. I am also grateful for his advices as a friend which make me think seriously about my career plans. Here I would also like to acknowlege the support of the office of naval research for funding the projects that I work on in the vortical flow research lab in MIT.

This thesis won't come out without Dr. Zhu's original idea and initial work on this topic. His paper list for the tutorial of FLEX3D and his initial development of the leading-edge separation idea helped me a lot. I would also like to thank Dr. Yuming Liu for his insight advices to continue my research work on this topic which finally comes out as my thesis. In addition, for his support as a friend, I can not express my gratitude enough.

I wish to take the chance here to thank my tutor and friend, Dr. Kelli Hendrickson. I really appreciate her kindness to help me in my research and in life. Since I started my research on steep breaking waves when I first arrived at MIT, she has been working with me as my tutor. She is tireless to answer my questions in details not only in research, but also in computer problems. Other than that, she shares her experience in MIT and in life with me. She is really a good friend and an elder sister to me in life. I also wish to thank Dr. Lian Shen. His physical insights and advices inspired me a lot when I did my first topic on the modeling of steep breaking waves. I really learned a lot from his way of how to do research and how to read papers. I am grateful to him not only because of his inspiration in my research work, but also advices as a sincere friend.

My sincere gratitude goes to my friends and labmates of vortical flow reseach lab for their help and kindness. They are Dr. Guangyu Wu, Dr. George Papaioanou, Dr. Benjamin Connell, Ms. Areti Kiara, Mr. Gabe Weymouth, Ms. Hongmei Yan, Mr. Mohammad-Reza Alam. Especially, I am grateful to Areti Kiara and Hongmei

3

Contents

List of Figures

10

11

12

13

List of Tables

Chapter 1

Introduction

1.1　Motivition

Many airborne or aquatic creatures have showed extraordinary propulsion efficiency and high maneuverability after millions of years of evolution. The performance of those creatures is far beyond that of current vehicles. Inspired by wings, fins or other appendages of those creatures for locomotion purposes, researchers begin to pay more and more attention to the oscillating foil which is the basic means of locomotion as propulsion/maneuvering devices on man-made vehicles (e.g., Anderson 1996; Anderson et al. 1998). It has been demonstrated in the literature that this bio-mimetic system has the potential to outperform conventional propulsion devices in terms of efficiency, maneuverability, and stealthiness (Triantafyllou et al. 1995). Oscillating foil has other exciting engineering applications such as wind/tidal power recovering machines (Campbell 2002).

Swimming efficiencies of fish and cetaceans have been found related to the Strouhal number and the range of the Strouhal number between 0.20 and 0.40 has been found associated with enhanced swimming efficiency for fish and cetaceans (Triantafyllou et al. 1991; Triantafyllou et al. 2000). It is similar for flying creatures (Wang 2000; Taylor et al. 2003).

To mimic the swimming and flying creatures, oscillating foil has been investigated. Extensive experiments have been conducted to illustrate the near-body flow features

around oscillating foils. By investigating vortical flow patterns in the wake of an NACA0012 airfoil pitching at small amplitudes in a low speed water channel at various Strouhal numbers, Koochesfahani (1989) showed the transition from the drag vortex wake (Von Karman vortex street) to a thrust wake (inversed Von Karman vortex street). It is the thrust wake that provides the propulsion.

It is found that for oscillating foils, optimal thrust can be achieved when the Strouhal number is in the range between 0.25 and 0.35 (Triantafyllou et al. 1991). Triantafyllou et al. (1995) found that efficiency was at its peak when the maximum angle of attack was between 15° and 25° for oscillating foil.

With both pitching and heaving motions included, Anderson discovered the relationship between the vortex pattern and the Strouhal number S_t and maximum angle of attack α_{max}(Anderson 1996; Anderson et al. 1998). Anderson' observations highlighted the significant influences of the leading-edge separations (LES) in the structure of the wake. For the moderate heave amplitude (heave to chord ratio=1.0), in order to avoid vortex shedding near the leading edge, either the range of attack angle has to be limited ($\alpha_{max} <\simeq 7^o$) or the Strouhal number must be small ($S_t <\simeq 0.12$) by visualizing the near-body flow field around a heaving-pitching foil. Beyond that domain, the leading-edge separation is distinguishably shown in the flow field. In fact within a large range of parameters ($0.3 < S_t < 0.5$ and $13^o < \alpha_{max} < 36^o$), the flow field is dominated by vortices generated near the leading edge. It is found that moderate formation of leading-edge vortices has been associated with high propulsive efficiency, up to 87% (Anderson et al. 1998).

The hydrodynamic performance of oscillating foils has also been measured and documented. By systematic experiments, Read (2000) mapped the thrust/lift forces and propulsion efficiency of an oscillating foil undergoing a combined heaving-pitching motion while translating forward over a wide range of kinematical parameters. Similarly, the hydrodynamic properties of a foil doing three-dimensional rolling-pitching motion have been investigated as well (Polidoro 2003).

16

1.2 A Review of Previous Work

Necessary theoretical and numerical investigations are needed to illustrate the physics of oscillating foils with leading-edge separations. Moreover, an accurate numerical model can also facilitate the optimizing designs of oscillating foil apparatus. Theodorsen (1935) solved the two-dimensional potential flow around an oscillating flat plate and developed an unsteady aerodynamic model in a closed form. For more complicated problems in the potential flow regime, both two-dimensional and three-dimensional cases are computationally resolved using boundary element methods (e.g., Katz 1991; Zhu *et al.* 2002). However, in most of these potential-flow models the shedding of vortices near the leading edge, which is found to play an important role in experiments, is neglected.

In order to accurately predict the hydrodynamic forces and moments on an oscillating foil, it is critical that vorticity shedding from both the leading and the trailing edge should be taken into account. Numerical models have been developed to study the fluid motion around foils in two-dimensional (Wang 2000) and three-dimensional oscillations (Liu *et al.* 1998; Liu and Kawachi 1998; Ramamurti and Sandberg 2002) by solving the Navier-Stokes equation. The simulations in their research, on the other hand, are computationally expensive and restricted to low Reynolds numbers. Advancements in panel methods can allow an integral boundary layer method to be incorporated into the panel methods (Curle 1967). We can do a separation analysis by this method. However, when the flow separation happens, this method will break down.

Because the curvature of the surface of the foil leading edge is finite, it is difficult to determine the separation location and the modeling of unsteady flow separations near the leading edge remains a challenge. Taneda (1977) has examined the unsteady motion of blunt bodies such as circular or elliptical cylinders. By visualizing the streakline and streamline patterns near the separation position on the body surface, he was able to show the process of flow leaving the boundary layer, which is the flow separation. Although it is difficult to pinpoint the exact location of the separation,

17

the results suggest that it occurs at highly localized positions. From these separation locations, vortex inside the boundary layer joins the outer flow in the form of continuous vortex sheets, which then roll up to form distinguishable vortices. This discovery rationalizes the potential-flow model of vortex separation as vortex sheets, even if the shedding occurs near the leading-edge area.

To include leading-edge separation in a potential-flow model, Katz (1981) proposed a method in which the vortex shedding from both the trailing and the leading edges are approximated as discrete vortices generated at one prescribed point near the leading edge. This approach was implemented to solve the steady motion of a thin cambered foil with a large angle of attack and the results agree qualitatively with experiments. However, this approach requires predetermination of the exact position of the leading-edge separation especially in unsteady flows, which is not available in most cases, because the separation position near the leading edge tends to move with time.

Encouraged by the discovery of the highly localized separation location by Taneda (1977) and the limited success of the approach by Katz (1981), we seek a leading-edge separation model that can be used for potential flow and thus the leading-edge separation can be modeled by a thin vortex sheet in the same way as the trailing-edge separation. Because the separation location is difficult to predict especially in unsteady flows, Zhu (private communication 2004) proposed that instead of modeling the leading-edge separation by a single leading-edge vortex sheet, we can consider a group of vortex sheets, each of them generated from a separation line. These separation lines are distributed within a separation region near the leading edge; the position of each of them is prescribed and fixed. The unsteady dynamics of the leading-edge separation is then modeled by the collective effects of these shear layers. In implementation, the shear layers can only be initiated from discontinuous edges of the body surface where the Kutta condition is applicable. Because there is no such discontinuities around the leading edge, a convenient way is to initiate the separation vortex sheets from the corners between neighboring panels.

However, for Zhu's proposal there are three difficulties.

18

- We have to specify the size of the separation area before each simulation because the size of the separation area may differ when the motion of the foil changes corresponding to different Strouhal numbers and maximum angles of attack.

- We need to decide the number of separation lines in the separation area. Because the separation lines are assumed to be the corner lines between neighboring panels, when we increase the number of panels on the foil surface the number of the separation lines will change and we may not obtain convergent results.

- The group of leading-edge vortex sheets may interact, which is problematic.

Further multiple vortex sheets are not supported by experiments. In general, only one or two vortex sheets are shed from the rounded leading edge (Taneda 1977). Therefore, we follow the approach that the leading-edge separation can be modeled by a single thin vortex sheet.

1.3   A Review of Main Work in This Thesis

To model the leading-edge separation by a thin vortex sheet, we consider a criterion for the location of separation. We did an extensive study of several criteria such as the angle of attack (Minotti 2002) and the Moore-Rott-Sears model (Moore 1958; Rott 1956; Sears 1975 and Williams 1977), which showed that the unsteady separation point is characterized by the simultaneous vanishing of the shear and the velocity at a point within the boundary layer as seen by an observer moving with the separation.

Finally we find that the most promising is the criterion of the local minimum of the pressure gradient, which is physically the starting point of the adverse pressure gradient. In implementation, we first compute the location of the local minimum of the pressure gradient near the leading edge of the foil without the leading-edge wake sheet. Then we simulate the oscillating foil with both trailing-edge and leading-edge wake sheets after the determination of the location of leading-edge separation. Because we predetermine the location for leading-edge separation at each time step, we can account for the moving separation point as well.

19

In present work we employ a boundary element approach to investigate the hydrodynamic loads on a three-dimensional foil undergoing translation and oscillation. Similar to the algorithm applied to simulate fish swimming (Zhu *et al.* 2002), in this numerical model the flow is calculated by solving a boundary-integral equation, with the effect of wakes modeled as shear layers originated from the sharp trailing edges. What is different is that we include the leading-edge separation model as stated above as well. The strength of these sheet layers are determined by imposing the Kutta condition. A low-order boundary element scheme is utilized to solve this initial boundary value problem.

Because of the Lagrange scheme of the wake relaxation in the boundary element simulation, the leading-edge wake sheet goes into or through the thin foil easily. This is not physical and it also causes numerical difficulties. To solve the problem of the wake penetration into the body, we present the pre-check technique in our simulation.

For the low-order boundary element method used for our simulation, we also made an important modification. We removed the dependence of our numerical results on a free parameter which controls the length of the first row of the trailing-edge wake panels by using a linear distribution of the singularities on the first row of the trailing-edge wake panels following Hsin (1990).

We apply our leading-edge separation model and the pre-check technique in our modified low-order boundary element method to examine the thrust and propulsion efficiency of a foil undergoing heave and pitch motions. Results show that for small maximum angle of attack ($\alpha_{max} < 15^o$), the problem can be resolved accurately by the low-order panel method without considering the effect of leading-edge vortices. For higher maximum angles of attack, however, the inclusion of the leading-edge separations significantly improve the performance of the algorithm compared to the experimental results of Read (2000).

1.4 Chapter Preview

The rest of the thesis is organized in the following way. In Chapter 2, we describe the physical problem, including the geometry of the foil and the kinematics of the motion and we highlight that the angle of attack profile can take several forms according to different parameter combinations, which can affect the thrust and efficiency greatly. In Chapter 3, the mathematical formulation is presented. The governing equations with boundary conditions and the wake model we use are specified. The formulas for the calculation of the thrust coefficient and propulsion efficiency are introduced. In Chapter 4, the low-order panel method with an important modification is presented. In Chapter 5, the modeling of the leading-edge separation is introduced. The location for the separation near the leading edge and the strength of the leading-edge separation are discussed. The problem of the penetration of the leading-edge wake sheet into the body is addressed. In Chapter 6, the convergence of our numerical model is examined. Further the performance of the model is discussed by comparing our numerical results with the experimental measurements by Read (2000) on the dynamics of heaving-pitching foils. The conclusion and further possible improvements for the leading-edge separation model are discussed in Chapter 7.

Chapter 2

Physical Problem

2.1 Equation of the Heaving-Pitching Motion

For comparison with the experiments (Read 2000), we consider the heaving-pitching motions of an NACA0012 foil with a constant straight forward speed U in the negative x direction as displayed in Figure 2-1. The heaving-pitching motions are prescribed. The NACA0012 foil used in the experiment has span $s = 0.6m$ and chord $c = 0.1m$. The towing speed U used in the experiment is $U = 0.40m/s$ corresponding to a Reynolds number of approximately $Re = \frac{Uc}{\nu} = 40000$, where ν is the kinematic viscosity in m^2/s. Both the heave and pitch motions are sinusoidal in time with the same frequency.

The heave motion as a function of time t is

$$h(t) = h_0 \sin(\omega t) \tag{2.1}$$

where h_0 is the heave amplitude in meters, ω is the frequency in radians/second and time t is in seconds.

The pitch motion is about the foil's 1/3 chord position. The pitch motion is then

$$\theta(t) = \theta_0 \sin(\omega t + \psi) \tag{2.2}$$

22
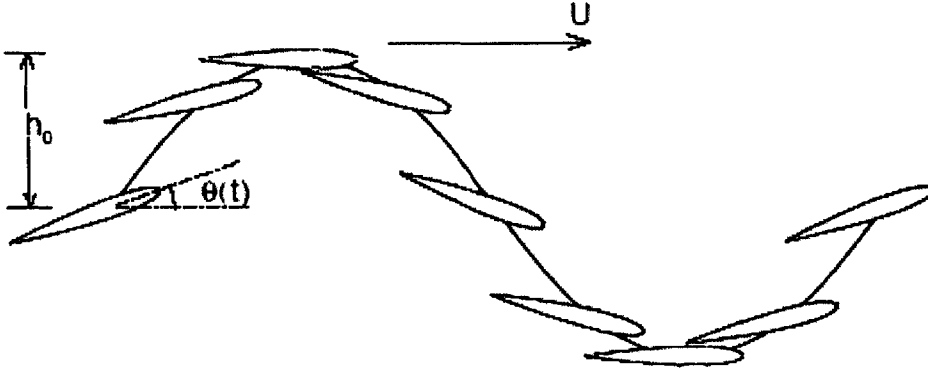
Figure 2-1: Heaving-pitching motion of an oscillating foil.

where θ_0 is the pitch amplitude in radians and ψ is the phase angle between pitch and heave in radians.

For a foil undergoing heaving-pitching motion, the angle of attack $\alpha(t)$ as a function of time t is

$$\alpha(t) = \arctan(\frac{\dot{h}(t)}{U}) - \theta(t) \tag{2.3}$$

where U is the forward velocity in meters/second and $\dot{h}(t)$ is the heave velocity as a function of time.

$$\dot{h}(t) = h_0 \omega \cos(\omega t) \tag{2.4}$$

For convenience, one of the most important parameters in this study, the Strouhal number, is introduced here, which is defined as

$$St = \frac{2h_0 f}{U} \tag{2.5}$$

where h_0 is the heave amplitude in meters, f is the frequency in Hz and U the forward speed in meters/second.

$2h_0$ is an estimate of the width of the foil wake. Since we do not know the width of the foil wake as a priori, $2h_0$ is an approximation. As to the parameter space

23

investigated in the experiment of a heaving-pitching foil by Read (2000), $2h_0$ is a valid estimate. The trailing edge excursion can also be used (Triantaffou *et al.* 1991 and 1993). However, the trailing edge excursion is a function of the test parameters. Therefore, the approximation of the width of the foil wake $2h_0$ is used for the definition of the Strouhal number.

2.2   Parametric Study

The parameters that describe the heaving-pitching motion are as follows:

- Strouhal number S_t

- Heave/chord ratio h_0/c

- Maximum angle of attack α_{max}

- Phase angle between the heave motion and pitch motion ψ

For foils with pitching and heaving motions, S_t is well known to govern the vortex growth and shedding regimes (Taylor *et al.* 2003, Anderson *et al.* 1998 and Wang 2000). Propulsive efficiency is high over a narrow range of S_t, usually in the range of $0.20 < S_t < 0.40$. In this range, enhanced swimming efficiency happens for fish and insects in nature. For oscillating foils, optimal thrust happens in the range of $0.25 < S_t < 0.35$ (Triantafyllou *et al.* 1991). Triantafyllou *et al.* (1995) found that efficiency reached its maximum when the maximum angle of attack is in the range of $15^o < \alpha_{max} < 25^o$. Therefore, in our simulation we take the parameter space of $0.20 < S_t < 0.40$ and $15^o < \alpha_{max} < 40^o$ to compare with the experiments by Read (2000).

The pitch amplitude θ_0 is calculated at a desired maximum angle of attack. For a given maximum angle of attack, there are two solutions of the pitch amplitude (Read 2000). The double solutions of the angle attack equation result from the fact that the foil can pitch up or down in respect to the positive or negative angle of attack. One solution will let the foil shed a thrust wake and the other will result in a drag

24

Table 2.1: Coefficients for the modified heave motion

Strouhal number	G_1	G_3	G_5
0.32	1.00000	0.02152	0.00063
0.36	1.00000	0.02553	0.00084
0.40	1.00000	0.02946	0.00107
0.44	1.00000	0.03326	0.00130
0.48	1.00000	0.03691	0.00154
0.52	1.00000	0.04039	0.00107
0.56	1.00000	0.04370	0.00201
0.60	1.00000	0.04684	0.00224

wake. The thrust wake shows a mean velocity profile excess like a jet similar to the reversed Von Karman street behind the foil (Read 2000). It will provide the foil a forward propulsion force. The drag wake exhibits a velocity deficit analogous to the Von Karman street behind a bluff body, which will result in a drag force on the foil (Drucker and Lauder 2002). Our interests are in the cases of the thrust wake that is produced by fish for propulsion.

If the phase angle ψ is 90° and the maximum angle of attack α_{max} appears only twice in one period, then the pitch amplitude θ_0 can be written as Equation (2.6). Otherwise we need to use Equation (2.3) to solve for θ_0.

$$\theta_0 = \arctan(\frac{h_0\omega}{U}) \pm \alpha_{max} = \arctan(S_t\pi) \pm \alpha_{max} \qquad (2.6)$$

where '+' corresponds to a drag wake and '−' corresponds to a thrust wake.

2.3   Angle of Attack Profile

It should be noted that the angle of attack profile can take several forms according to different parameter combinations. The angle of attack may reach the maximum value more than twice over one period, while heave and pitch maxima occur only twice per period. This multi-peaked profile tends to appear at higher Strouhal numbers (Read 2000).
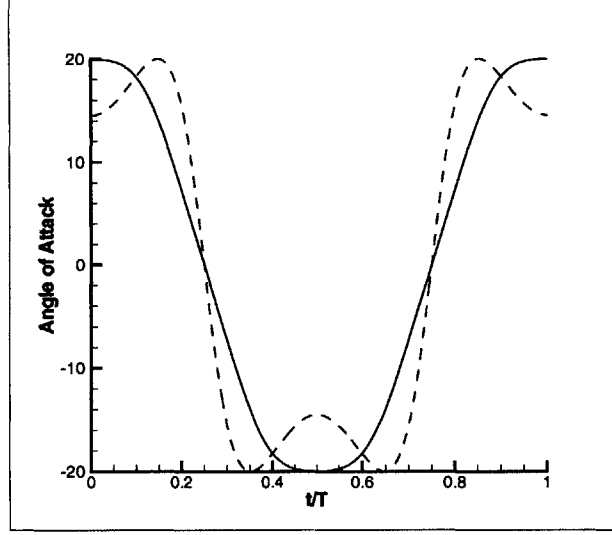
Figure 2-2: Recovery of the sinusoid profile of angle of attack.
Dashed: pitch motion as Equation (2.2) and heave motion as Equation (2.1),
Solid: pitch motion as Equation (2.2)and modified heaving motion as Equation (2.7).
The parameters are: U=0.4 m/s, S_t = 0.60, h_0/c = 1.0, α_{max} = 20°, ψ = 90°,
G_1,G_2,G_3 as in Table 2.1.

The thrust for a given set of parameters tends to decrease when the angle of attack

profile takes on the forms of more than two peaks over one period. In order to recover

the performance of the higher Strouhal numbers, the sinusoid profile of angle of attack

needs to be recovered. Read (2000) achieved this by altering the heave motion in such

a way that the higher order harmonics in $\arctan(\frac{h_0\omega\cos(\omega t)}{U})$ are cancelled and the two-

peak profile of the angle of attack is obtained. The heave motion is altered by adding

higher order terms so that the heave as a function of time t becomes:

$$h(t) = h_0[G_1\sin(\omega t) + G_3\sin(3\omega t) + G_5\sin(5\omega t)] \qquad (2.7)$$

and the heave velocity is:

$$\dot{h}(t) = h_0\omega[G_1\sin(\omega t) + 3G_3\sin(3\omega t) + 5G_5\sin(5\omega t)] \qquad (2.8)$$

where G_1,G_3,G_5 can be found in Table 2.1 for the range of Strouhal numbers from

0.32 to 0.60.

26

Figure 2-2 shows the recovery of the sinusoid profile of angle of attack by altering the heave motion. Because of the modified heave motion, we need to resolve the pitch amplitude again to obtain the desired maximum angle of attack.

The new higher order heave motion changes only slightly. However, a large change appears in the profile of angle of attack, which results in a great effect on the performance of the thrust (Read 2000).

Chapter 3

Mathematical Formulation

The flow field around the three-dimensional foil is assumed to be irrotational and incompressible. The body is modeled as a closed surface S_b. The viscous effect is modeled by a thin shear wake sheet which is shed from the sharp trailing edge and another wake sheet shed from the rounded leading edge. Except for the wake sheets, the fluid is assumed to be invicid. Then for any point $\mathbf{x} = (x, y, z)$ in the fluid, the flow field can be described by the velocity potential $\Phi(\mathbf{x}, t)$ which satisfies the Laplace equation, together with the no-flux boundary condition on the surface of the body S_b and a radiation condition that $\Phi(\mathbf{x}, t)$ decays rapidly to zero in the far field boundary S_∞.

Following Zhu *et al.* (2002), the total potential $\Phi(\mathbf{x}, t)$ can be written as a linear superposition of a body perturbation velocity potential $\Phi_b(\mathbf{x}, t)$ and a wake perturbation velocity potential $\Phi_w(\mathbf{x}, t)$, each satisfying the Laplace equation. The wakes are modeled by thin shear layers S_w which are represented by the distribution of dipoles.

3.1   Governing Equation

The boundary value problem can be formulated. $\Phi(\mathbf{x}, t)$ satisfies the Laplace equation within the fluid and radiation condition in the far field. The no-flux boundary condition on the surface of the body is imposed as

28

where $\gamma = 2\pi$ if $\mathbf{x}$ is on the surface of the foil, and $\gamma = 4\pi$ if $\mathbf{x}$ is in the fluid.

Thus for $\mathbf{x}$ on the surface of the foil, Equation (3.4) becomes

$$-2\pi\Phi_b(\mathbf{x}, t) + \int\int_S (\frac{1}{r}\nabla\Phi(\mathbf{x}', t) - \Phi(\mathbf{x}', t)\nabla(\frac{1}{r})) \cdot \mathbf{n}dS' = 0 \qquad (3.6)$$

where $S = S_b + S_w + S_\infty$, $r = |\mathbf{x} - \mathbf{x}'|$ is the distance from the point $\mathbf{x}' \in S$ to the field point $\mathbf{x}$.

It can be written as

$$-2\pi\Phi_b(\mathbf{x}, t) + \int\int_S \Phi(\mathbf{x}', t)\frac{\partial(1/r)}{\partial n}dS' = \int\int_S 1/r\frac{\partial\Phi(\mathbf{x}', t)}{\partial n}dS' \qquad (3.7)$$

Since the singularities in the integrands decay as $1/r$ or $1/r^2$ when $r \to \infty$, and thus fullfill the boundary condition at S_∞ automatically. At the wake boundary S_w, we have $\frac{\partial\Phi(\mathbf{X}, t)}{\partial n} = 0$ since the normal velocity of the fluid is continuous across the thin wake shear layer. Then the final mathematical equation for our simulation is

$$-2\pi\Phi_b(\mathbf{x}, t) + \int\int_{S_b+S_w} \Phi(\mathbf{x}', t)\frac{\partial(1/r)}{\partial n}dS' = \int\int_{S_b} 1/r\frac{\partial\Phi(\mathbf{x}', t)}{\partial n}dS' \qquad (3.8)$$

The boundary value problem, involving both the body influence potential Φ_b and the wake influence potential Φ_w, is solved this way here. Φ_b and Φ_w are decomposed and the only unknowns are the strengths of the body influence potential Φ_b. At any time step t, the boundary value problem for $\Phi_b(\mathbf{x}, t)$ is determined with the known wake potential from the previous time step except for the most recently shed portion of the wake sheet. The unknown strength of the newest portion of the wake sheet can be represented by the body velocity potential through the Kutta condition. Thus, only the strengths of the body velocity potential are unknown variables in the equation. After the body velocity potential is solved, the wake velocity potential of the newly-shed portion of the wake sheet can be calculated. Then the flow field at the time step t will be determined by the body influence potential $\Phi_b(\mathbf{x}, t)$ and the wake influence potential $\Phi_w(\mathbf{x}, t)$.

30

3.2 Time-stepping Wake Model

The Kutta condition is used as a boundary condition to determine the strength of the doublets to be shed into the first row of the wake. At each new time step, a new row of wake is added to the wake sheet. At the first time step, no wake exists for the first solution, which corresponds to an impulsively started object. On the subsequent time steps, a new row of the wake is added to each wake at the wake separation line and the remaining rows of the wake are convected downstream with the local velocity.

The Kutta condition states that the velocity at the rear stagnation point must be finite. When two or more vortex lines coincide, the strength of the resulting vortex line is equal to the sum of the strengths of the individual vortex lines so that the resultant strength of the vortex line along the separation line would be zero to satisfy the Kutta condition. Therefore, the strength of the vortex ring on the newly-shed rows of the wake sheets is equal to the difference of the strengths in velocity potential of the two surface panels near the separation line, in order to cancel the strength of the vortex line along the separation line. On the other hand, the strengths of the remaining rows of the wake are known from the previous time step. With the inviscid assumption, the strengths of the remaining rows of the wake will stay constant. In our leading-edge separation model, the Kutta condition is also used for the vortex sheet shed near the leading-edge, which represents the leading-edge separation.

In our simulation the first row of the wake panels is shed from the separation line at time $t = 0$ without initially specified wake, which corresponds to an impulsively started foil. Alternatively, an initial wake may be prescribed to simulate a steady-state condition. Then the initial wake cannot be time-stepped to further its development. This is corresponding to the time-stepping at some time $t > 0$.

This is the time-stepping wake model used in the simulation, which can determine the position and strength of the wake once it is shed into the flow field.

$$\frac{\partial \Phi(\mathbf{x}, t)}{\partial \mathbf{n}} = \mathbf{V}_b(\mathbf{x}, t) \cdot \mathbf{n} \tag{3.1}$$

where $\mathbf{V}_b$ is the prescribed body motion and $\mathbf{n}$ is the unit normal vector of the body surface pointing into the body.

By applying Green's Theorem, we can write the velocity potential $\Phi(\mathbf{x}, t)$, which is a linear superposition of a body perturbation velocity potential $\Phi_b(\mathbf{x}, t)$ and a wake perturbation velocity potential $\Phi_w(\mathbf{x}, t)$, in terms of surface integral over the body surface S_b, the wake surface S_w and the boundary at infinity S_∞

$$\int\int_S (\frac{1}{r}\nabla\Phi(\mathbf{x}', t) - \Phi(\mathbf{x}', t)\nabla(\frac{1}{r})) \cdot \mathbf{n} dS' = 0 \tag{3.2}$$

where $S = S_b + S_w + S_\infty$, $r = |\mathbf{x} - \mathbf{x}'|$ is the distance from the point $\mathbf{x}' \in S$ to the field point $\mathbf{x}$.

Following the derivation of Katz and Plotkin (1991), for a particular point $\mathbf{x}$ surrounded by a small sphere of radius ϵ inside the fluid region, Equation (3.2) becomes:

$$\int\int_{S+sphere\ \epsilon} (\frac{1}{r}\nabla\Phi(\mathbf{x}', t) - \Phi(\mathbf{x}', t)\nabla(\frac{1}{r})) \cdot \mathbf{n} dS' = 0 \tag{3.3}$$

To evaluate the integral over the small sphere, we introduce a spherical coordinate system and then the normal vector $\mathbf{n}$ is $\mathbf{n} = -e_r$. Thus $\mathbf{n} \cdot \nabla\Phi = -\partial\Phi/\partial r$ and $\nabla(1/r) = -(1/r^2)e_r$. Equation (3.3) then becomes

$$-\int\int_{sphere\ \epsilon} (\frac{1}{r}\frac{\partial\Phi(\mathbf{x}', t)}{\partial r} + \frac{\Phi(\mathbf{x}', t)}{r^2})dS' + \int\int_S (\frac{1}{r}\nabla\Phi(\mathbf{x}', t) - \Phi(\mathbf{x}', t)\nabla(\frac{1}{r})) \cdot \mathbf{n} dS' = 0 \tag{3.4}$$

As $\epsilon \rightarrow 0$, the derivative of the velocity potential vanishes since we assume the velocity potential and its derivatives are well-behaved functions and thus do not vary much in a very small sphere. Then

$$-\int\int_{sphere\ \epsilon} (\frac{1}{r}\frac{\partial\Phi(\mathbf{x}', t)}{\partial r} + \frac{\Phi(\mathbf{x}', t)}{r^2})dS' = -\int\int_{sphere\ \epsilon} \frac{\Phi(\mathbf{x}', t)}{r^2}dS' = -\gamma\pi\Phi(\mathbf{x}, t) \tag{3.5}$$

3.3 Propulsive Forces and Efficiency

At each time, after the governing equations are solved, the total flow potential $\Phi(\mathbf{x}, t)$ is known. The pressure coefficient $c_p(\mathbf{x}, t)$ at each surface panel can be found by the unsteady Bernoulli equation.

$$c_p(\mathbf{x}, t) = -\frac{1}{U^2}(\nabla\phi(\mathbf{x}, t) \cdot \nabla\phi(\mathbf{x}, t) + 2\frac{\partial\phi(\mathbf{x}, t)}{\partial t}) \tag{3.9}$$

where U is the forward speed of the foil.

The hydrodynamic force $\mathbf{F}$ can be found by integrating the pressure p over the body surface S_b.

$$\mathbf{F} = \frac{1}{2}\rho U^2 \int\int_{S_b} c_p \mathbf{n} dS = -\rho \int\int_{S_b} (\frac{1}{2}\nabla\phi(\mathbf{x}, t) \cdot \nabla\phi(\mathbf{x}, t) + \frac{\partial\phi(\mathbf{x}, t)}{\partial t})\mathbf{n} dS \tag{3.10}$$

where ρ is the density of the water.

For a heaving-pitching motion, the hydrodynamic force $\mathbf{F}$ has two components: the thrust force F_x in the horizontal direction and the lifting force F_z in the vertical direction. We can further improve the prediction of the thrust force by subtracting an approximation of the friction drag from it.

$$\mathbf{F}'_x = \mathbf{F}_x - \frac{1}{2}C_d \rho cs U \mathbf{U} \tag{3.11}$$

where C_d is the friction coefficient on a fixed foil with zero angle of attack and forward speed U, ρ is the density of the water, c is the chord of the foil and s is the span of the foil.

An estimate of C_d is

$$C_d = 2C_{fd}(1 + 2\tau + 60\tau^4) \tag{3.12}$$

where

$$C_{fd} = 2.656/\sqrt{R_e} \tag{3.13}$$

where R_e is the Reynolds number based on the chord length and τ is the thickness

to chord ratio of the foil.

As to the NACA0012 foil used in our simulation, $\tau = 0.12$. Zhu (private communication 2004) found that in most cases the contribution from the friction is less than 3 % of the total hydrodynamic force.

The time average thrust coefficient is defined as

$$C_t = \overline{F'_x}/\frac{1}{2}\rho c s U^2 \tag{3.14}$$

where $\overline{F'_x}$ is the time average thrust.

At a certain time step, the input power P, defined as the rate of energy transmission to the fluid, can be obtained as

$$P = -\rho \int \int_{S_b} (\frac{1}{2}\nabla\phi(\mathbf{x},t) \cdot \nabla\phi(\mathbf{x},t) + \frac{\partial\phi}{\partial t})\mathbf{V}_b \cdot \mathbf{n}ds \tag{3.15}$$

Finally, the propulsive efficiency η is defined as

$$\eta = U\overline{F'_x}/\overline{P} \tag{3.16}$$

where U is the forward speed, $\overline{F'_x}$ is the time average thrust, $\overline{P}$ is the time average input power.

Chapter 4

Numerical Method

In order to accurately predict the hydrodynamic forces and moments on an oscillating foil, it is critical that vorticity shedding from both the leading and the trailing edge should be taken into account. Numerical models have been developed to study the fluid motion around foils in two-dimensional (Wang 2000) and three-dimensional oscillations (Liu et al. 1998; Liu and Kawachi 1998; Ramamurti and Sandberg 2002) by solving the Navier-Stokes equation. The simulations in their research, on the other hand, are computationally expensive and restricted to low Reynolds numbers. Therefore, following Zhu et al. (2002), we solve the governing equations with the boundary conditions by a low-order panel method in order to obtain the body influence potential ϕ_b and then obtain the hydrodynamic forces and moments.

This chapter is organized this way. In Section 4.1, we present the formulation of the low-order panel method. We show the discretization of the governing equation and the paneling of the foil surface. Furthermore, we discuss the independence of the numerical results on the desingularization factors. In addition, the method to smooth the transition of an impulsively started foil is specified, and the calculation of the fluid velocity on the foil surface and the unsteady pressure is introduced. In Section 4.2, our modification of the low-order panel method is presented. The dependence of the numerical results on a free numerical parameter is removed. Section 4.3 summarizes this chapter.

4.1 Formulation of the Low-Order Panel Method

In the low-order panel method, both the body surface S_b and the wake sheets S_w are discretized into finite numbers of quadruple panels (Katz 1991). Over each panel the singularities are distributed with constant strengths at the collocation points. To increase the accuracy of prediction of the unsteady flow field, smaller panels are used in the regions of presumed rapid potential variation, such as the regions of the large curvature of the foil.

Advancements in panel methods can allow an integral boundary layer method to be incorporated into the panel methods (Curle 1967). We can do a separation analysis by this method. However, when the flow separation happens, this method will break down. Therefore, we modeled the leading-edge separation in the same manner as the trailing-edge separation. The details about the leading-edge separation model will be discussed in Chapter 5.

4.1.1 Discretization of the Governing Equation

After discretizing and breaking the integrals up into surface integrals over each panel of the constant strength velocity potential, the integral equation becomes a set of linear equations to be solved for the unknown strengths of the surface velocity potential. At any time t, the set of linear equations of $\Phi_b(\mathbf{x}_i, t)$ at each panel collocation point $\mathbf{x}_i$ are

$$-2\pi\Phi_b(\mathbf{x}_i, t) + \sum_{j=1, j\neq i}^{N_b} (\Phi_b(\mathbf{x}_j, t)C_{ij}) + \sum_{k=1}^{N_w}(\Phi_w(\mathbf{x}_k, t)C_{ik}) = \sum_{j=1}^{N_b}(\frac{\partial\Phi_b(\mathbf{x}_j, t)}{\partial n}B_{ij}) \quad (4.1)$$

where N_b is the total number of the body surface panels, N_w is the total number of the wake panels. C_{ij}, C_{ik}, B_{ij} are body influence coefficients, wake influence coefficients and the normal velocity influence coefficients for the velocity potential, given by the following:

$$C_{ij} = \int\int_{S_b} \frac{\partial 1/r_{ij}}{\partial n}dS \quad (4.2)$$

$$C_{ik} = \int\int_{S_w} \frac{\partial 1/r_{ik}}{\partial n} dS \tag{4.3}$$

$$B_{ij} = \int\int_{S_b} \frac{1}{r_{ij}} dS \tag{4.4}$$

where $r_{ij} = |\mathbf{x}_i - \mathbf{x}_j|$, $r_{ik} = |\mathbf{x}_i - \mathbf{x}_k|$.

The right side of Equation (4.1) is known by applying the kinematic boundary condition below for each panel on the body surface.

$$\frac{\partial \Phi_b(\mathbf{x}_i, t)}{\partial n} = \mathbf{V}_b(\mathbf{x}_i, t) \cdot \mathbf{n} \tag{4.5}$$

where $\mathbf{V}_b(\mathbf{x}_i, t)$ is the prescribed body motion on each panel and $\mathbf{n}$ is the unit normal vector of the body surface pointing into the body.

$\Phi_w(\mathbf{x}_k, t)$ is known from the previous time step by the time-stepping wake model, except at the first row of the wake panels. $\Phi_w(\mathbf{x}_k, t)$ for the first low of the wake panels is related to $\Phi_b(\mathbf{x}_i, t)$ through the Kutta condition. Thus the unknowns are only $\Phi_b(\mathbf{x}_i, t)$. The set of linear equations for $\Phi_b(\mathbf{x}_i, t)$ can be expressed in the general form

$$[\tilde{Q}]\Phi_b = [\tilde{P}] \tag{4.6}$$

where $\tilde{Q}$ is the influence matrix, Φ_b is the unknown body velocity potential and $\tilde{P}$ is the influence of the kinematic boundary condition and the existing wake sheets.

$\Phi_b(\mathbf{x}_i, t)$ and $\Phi_w(\mathbf{x}_k, t)$ can be obtained by an iterative scheme. At each time step, this set of linear equations is solved with the Kutta condition to obtain the body velocity potential $\Phi_b(\mathbf{x}_i, t)$. Then the unknown strengths for the first row of the wake panels can be obtained by Kutta condition and after that, the wake is updated and convected downstream with the local flow velocities. Therefore, As a result of this scheme, the total number of wake panels N_w will increase with time, while the total number of body panels N_b will remain a constant.
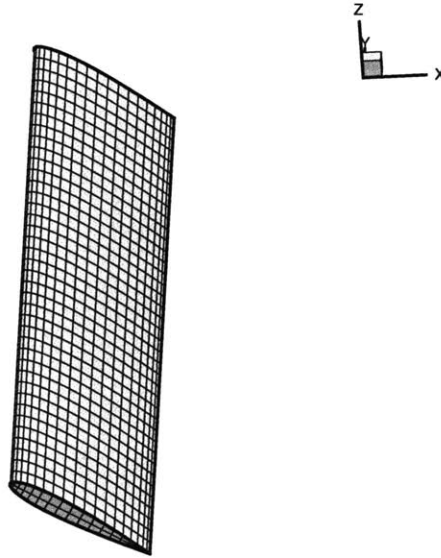
Figure 4-1: Panelling of the foil surface.

4.1.2   Paneling of the Foil Surface

To increase the accuracy of prediction of the unsteady flow field, smaller panels are used in the regions of presumed rapid potential variation, such as the regions of the large curvature of the foil. It is demonstrated that more accurate velocity values can be achieved by cosine paneling of the surface panels (Letcher 1989; Terzi and Chiu 1997) since near both the leading edge and the trailing edge of the foil, presumed rapid potential variation happens because of the large curvature of the foil. Letcher (1989) also showed that the highly accurate and stable drag predictions can be obtained by the trefftz-plane analysis of the far field wake, even from quite coarse panelizations. In our simulation both the cosine spacing of the foil surface and the trefftz-plane analysis are applied. The example of the paneling in our simulation is shown in Figure 4-1.

4.1.3 Short Transient Time of Impulsively Started Foil

We simulate the heaving-pitching foil with a constant straight forward speed U. Because we treat the foil as an impulsively started object, there is a short transient time period. Therefore, we present and analyze our results after this transient time. However, in this short transient time, the resulting forces are not smooth. Therefore, we try to smooth the transition. Weymouth (2005) used a ramping function to smooth the transition of the heaving-pitching ship motion in his simulation to minimize the transient response. However, we find that there is still some non-smoothness in our simulation by using a ramping function. Here we use a sinusoidal function $f(t)$ to smooth the transition from the initial conditions of the impulsively started foil. The prescribed translation, heave and pitch motions in the transient time are defined by the following:

$$U_{trans} = f(t)U \tag{4.7}$$

$$h_{trans}(t) = f(t)h_0 \sin(\omega t) \tag{4.8}$$

$$\theta_{trans}(t) = f(t)\theta_0 \sin(\omega t + \psi) \tag{4.9}$$

where

$$f(t) = \frac{1}{2}(1 - \cos(\frac{\pi}{N\Delta t}n\Delta t)) \tag{4.10}$$

N is total time step for the transient time, and n is the time step $(n < N)$.

We found that by using the sinusoildal smooth function, the transient time has to be greater than one period to remove the non-smoothness.

4.1.4 Desingularization

There are two desingularization factors used in our simulation, which are the wake desingularization factor δ_w and the body desingularization factor δ_b.

38

Wake Desingularization Factor δ_w

The material surface of the wakes is modeled by the thin shear layers which can be deformed freely and can not sustain normal stresses. It is convected downstream with the local velocities. The local velocity is usually determined by the Biot-Savart law after the body velocity potential Φ_b and the wake velocity potential Φ_w are determined, as Equation (4.11) shows.

$$\mathbf{v}(\mathbf{x}) = \frac{\Gamma}{4\pi} \oint \frac{\mathbf{s} \times \mathbf{r}}{r^3} dl \qquad (4.11)$$

where Γ is the circulation strength of the vortex ring, $\mathbf{s}$ is the tangent vector to the vortex element on the panel, $\mathbf{r}$ is the vector with magnitude r from the vortex element to the field point $\mathbf{x}$, and the path of the integration is along the sides of the panel.

However, the desingularization is necessary since the velocities of the corner points of the wake panels are calculated to convect the wake downstream and the corner points are on the edges of the wake panels. The wake vortex ring of strength Γ on a quadrilateral wake panel is assigned a core radius δ_w, which removes the singularities of the infinitesimally thin vortex sheet. The velocity induced at $\mathbf{x}$ by the wake vortex ring made of the panel edges can be expressed by the desingularized Biot-Savart law:

$$\mathbf{v}(\mathbf{x}) = \frac{\Gamma}{4\pi} \oint \frac{\mathbf{s} \times \mathbf{r}}{r^3 + \delta_w{}^3} dl \qquad (4.12)$$

As $\mathbf{x}$ approaches the vortex ring, r approaches zero and the velocity field expressed by Equation (4.12) approaches a finite limit.

Body Desingularization Factor δ_s

Similar to the wake panels, the body panels are desingularized with a core radius δ_s. When the desingularization is used in the calculation of the velocity field on the surface of the foil, this desingularization can stabilize the solution if fine mesh discretizations for the body surface are used for a complex boundary value problem. When the desingularization is used in the calculation of the velocity field very

near the body surface in the situation where the upstream vorticity impinges on the downstream body, non-physical free wake acceleration and deformation are avoided. Without this body desingularization, the wake shed at the leading edge of the body may convect into the body very easily, which will cause numerical difficulties in the boundary element simulation.

The desingularization of the wake and body panels is to imitate the effect of the viscosity in a real fluid by the finite thickness vortex rings; it eliminates the associated ill-posed problem of the dynamic evolution of the shear layers (Zhu private communication 2004).

Independence of Simulation Results on Desingularization Factors

Our simulation results do not depend on these two desingularization factors, the wake desingularization factor δ_w and the body desingularization δ_s, as long as these two desingularization factors are small enough. We did an extensive investigation into how to determine the non-dependence of our numerical simulation results on these two desingularization factors. If both desingularization factors are small enough, the resulting forces won't change when we vary the desingularization factors. The details about the independence on the two desingularization factors can be found in Section 6.4. Because the two desingularization factors are only used in the calculation of the velocities in the flow field, We compared the normal velocity of the fluid on the foil surface calculated by Equation (4.12) and the normal velocity of the foil surface, which is prescribed because of the prescribed motion of the foil. These two normal velocities should be the same because of the boundary condition. We find that from Figure 4-2 these two normal velocities compare well, except near the trailing edge of the foil. The mismatch near the trailing edge is because of the linear Kutta condition used in our simulation (Hess 1990).
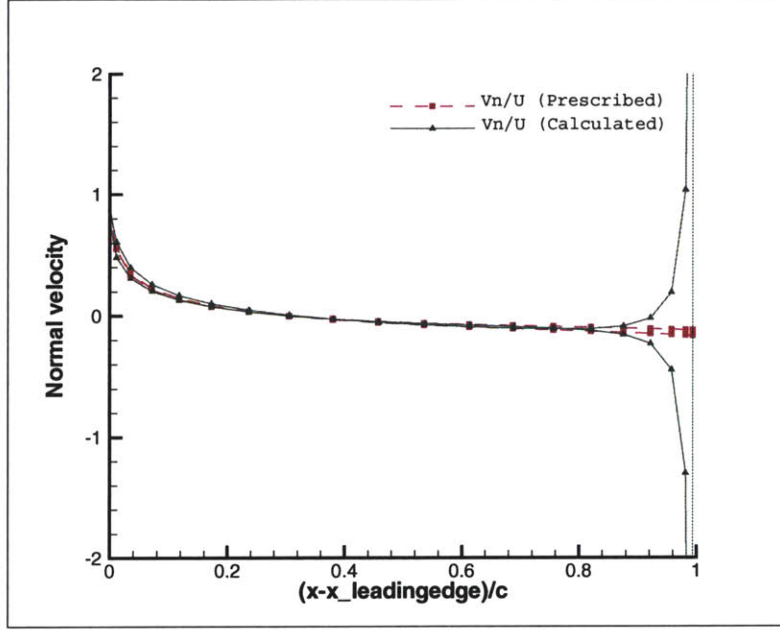
Figure 4-2: Comparison of the calculated and prescribed normal velocity on the foil surface at time $t/T = 1.25$. The parameters are: U=0.4 m/s, $S_t = 0.20$, $h_0/c = 0.75$, $\alpha_{max} = 30^o$, $\psi = 90^o$.

4.1.5 Calculation of Velocity on Foil Surface

The tangential velocity of the fluid on the body surface, which is used to compute the pressure and forces on the body, is computed by the second-order finite difference of the velocity potential on the body surface. However, we cannot calculate the tangential velocity at the panels neighboring the separation line by the second order finite difference. The tangential velocity calculated by one-side finite difference is not accurate since near the leading edge the velocity changes dramatically. Then the calculation of the velocity is not accurate and hence the pressure calculated is not accurate. From Equation (4.13), we can see the contribution of the term, which is associated with the tangential velocity, to the pressure . The contribution from the normal velocity term is fixed because the normal velocity of the fluid on the foil is the same as that of the foil, which is prescribed.

$$C_p = \frac{2}{U^2}\frac{\partial \phi}{\partial t} - \frac{v_t^2}{U^2} - \frac{v_n^2}{U^2} \qquad (4.13)$$

41

where v_t is the tangential velocity of the fluid on the foil surface and v_n is the normal velocity of the fluid on the foil surface.

Therefore, we compute the velocity near the leading-edge separation line by the equation derived from Green's Theorem.

$$\mathbf{v}(\mathbf{x}, t) = \mathbf{v}_\infty - \frac{1}{2\pi} \int \int_{S_b} \Phi_b(\mathbf{x}', t) \nabla(\mathbf{n} \cdot \nabla(\frac{1}{r})) dS' - \frac{1}{2\pi} \int \int_{S_w} \Phi_w(\mathbf{x}', t) \nabla(\mathbf{n} \cdot \nabla(\frac{1}{r})) dS'$$

$$-\frac{1}{2\pi} \int \int_{S_b} \nabla(\frac{1}{r}) \frac{\partial \Phi_b(\mathbf{x}', t)}{\partial n} dS' \tag{4.14}$$

Equation (4.14) can be written in the discretized form as:

$$\mathbf{v}(\mathbf{x}_i, t) = \mathbf{v}_\infty - \frac{1}{2\pi} \sum_{j=1}^{N_b} (\Phi_b(\mathbf{x}_j, t) V_{ij}) - \frac{1}{2\pi} \sum_{k=1}^{N_w} (\Phi_w(\mathbf{x}_k, t) V_{ik}) - \frac{1}{2\pi} \sum_{j=1}^{N_b} (\frac{\partial \Phi_b(\mathbf{x}_j, t)}{\partial n} P_{ij})$$

$$\tag{4.15}$$

where N_b is the total number of body surface panels and N_w is the total number of wake panels. V_{ij}, V_{ik} and P_{ij} are body influence coefficients, wake influence coefficients and the normal velocity influence coefficients for the velocity respectively, and defined below.

$$V_{ij} = \int \int_{S_b} \nabla(\frac{\partial 1/r_{ij}}{\partial n}) dS \tag{4.16}$$

$$V_{ik} = \int \int_{S_w} \nabla(\frac{\partial 1/r_{ik}}{\partial n}) dS \tag{4.17}$$

$$P_{ij} = \int \int_{S_b} \frac{\partial 1/r_{ij}}{\partial n} dS \tag{4.18}$$

where $r_{ij} = |\mathbf{x}_i - \mathbf{x}_j|$, $r_{ik} = |\mathbf{x}_i - \mathbf{x}_k|$.

42

4.1.6 Calculation of Unsteady Pressure

The unsteady part of the pressure $\frac{\partial \Phi(\mathbf{X},t)}{\partial t}$ is computed by a second-order backward difference scheme:

$$\frac{\Delta \Phi(\mathbf{x}, t_n)}{\Delta t} = \frac{4\Phi(\mathbf{x}, t_n) - 3\Phi(\mathbf{x}, t_{n-1}) + \Phi(\mathbf{x}, t_{n-2})}{2\Delta t} \qquad (4.19)$$

where n is the time step index.

Then the unsteady forces acting on the foil are calculated by integrating the unsteady pressure distribution over the surface of the foil.

4.2 Modification of the Low-Order Panel Method

In this section, we identify a free parameter in the numerical scheme of the low-order panel method and remove the dependence of our numerical results on the free parameter which controls the length of the first row of the trailing-edge wake panels by using a linear distribution of the singularities on the first row of the trailing-edge wake panels.

4.2.1 A Free Parameter in Low-Order Panel Method

The fluid velocity at the trailing edge with which the trailing-edge wake sheet is shed cannot be determined. According to potential theory the trailing edge is a stagnant point. In practice, the panel length L_{T1} of the first row of the trailing-edge wake, shown in Figure 4-3, depends on the time step Δt and a free parameter C_1 by $L_{T1} = C_1 U \Delta t$. We find that, for the low order panel method, the resulting forces will depend on the free parameter C_1 and the time step Δt. As the time step decreases, convergence cannot be achieved. C_1 is usually calibrated by experiments when there is only trailing-edge wake. For different motions of the oscillating foil, C_1 should be different.

In our simulation, which includes the leading-edge separation as well, the leading-edge wake is implemented in the same way as the trailing-edge wake and thus we
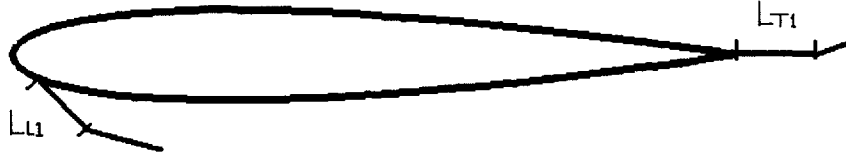
Figure 4-3: The panel length L_{T1} of the first row of the trailing-edge wake and the panel length L_{L1} of the first row of the leading-edge wake.

may need another parameter C_2 to control the panel size L_{L1} of the first row of the leading-edge wake panels by $L_{L1} = C_2 U \Delta t$. However, because the leading edge is not a sharp edge and the separation location near the leading edge is not a stagnant point, the fluid velocity at the separation location is different from that of the foil at the separation location. The velocity with which the leading-edge wake sheet is shed can be determined by the local velocity near the separation point by $L_{L1} = V_{sep} \Delta t$, where V_{sep} is the local velocity near the separation point.

Therefore, only one free parameter C_1, which controls the panel length of the first row of the trailing-edge wake panels, remains to be determined.

4.2.2 Convergence Problem

Now we consider only the trailing-edge separation to investigate the free parameter C_1. The convergence cannot be achieved because of the free parameter C_1. Using a constant C_1 and different sizes of time step, we obtain Figure 4-4 by simulating a heaving and pitching foil with only trailing-edge wake. $C_1 = 0.3$ is used in the simulation as a calibrated value. Here U and ΔX_T are fixed, where U is the forward speed and ΔX_T is the panel size of the foil surface panel nearest to the trailing edge. We can see from Figure 4-4 that convergence can not be obtained if we decrease the time step. The test case in Figure 4-4 has the following parameters: Forward speed $U = 0.4$ m/s, Strouhal number $S_t = 0.30$, maximum angle of attack $\alpha_{max} = 10^o$, heave/chord ratio $h_0/c = 0.75$ and the phase angle between the heave motion and pitch motion $\psi = 90^o$.

44
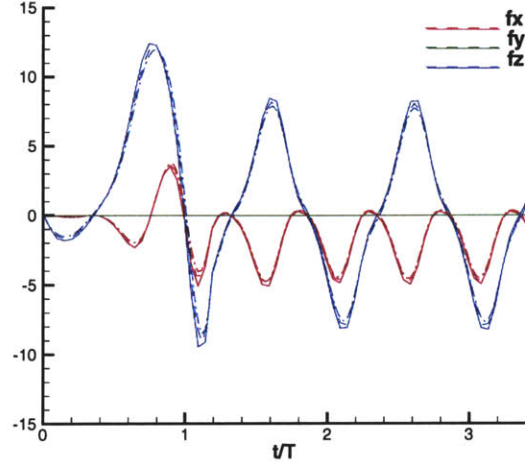
Figure 4-4: Non-convergence of the low order panel method with the constant distribution of velocity potential on the first row of the wake panels. Solid: $\frac{U\Delta t}{\Delta X_T} = 40$, Dashed: $\frac{U\Delta t}{\Delta X_T} = 30$, Dashed-dot: $\frac{U\Delta t}{\Delta X_T} = 20$. The parameters are: $U = 0.4$ m/s, $S_t = 0.30$, $h_0/c = 0.75$, $\alpha_{max} = 10^o$, $\psi = 90^o$.

For the same test case as in Figure 4-4, we can see the thrust coefficient and efficiency are dependent on C_1 from Figure 4-5 if we vary C_1 and keep the time step unchanged. There is no range of C_1 in which the thrust coefficient and the propulsion efficiency are almost constants. Near $C_1 = 0.3$, which is the calibrated value, if C_1 changes a little, the resulting thrust and efficiency will change greatly. Therefore, the value of C_1 is important for obtaining accurate thrust and efficiency values.

4.2.3 Removal of the Dependence on the Free Parameter C_1

To solve this non-convergence problem, we follow Hsin (1990) and obtain convergence by using linear distribution of the singularities on the first row of wake panels. On other rows of the wake panels the constant distribution of the singularities is kept.

By this modification, the results become independent of the time step and the panel size. Thus the dependence on the free parameter C_1 is removed. Figure 4-6 shows the convergence when the time step is decreased by using the linear distribution of the velocity potential on the first row of the wake panels. Hsin (1990) found no
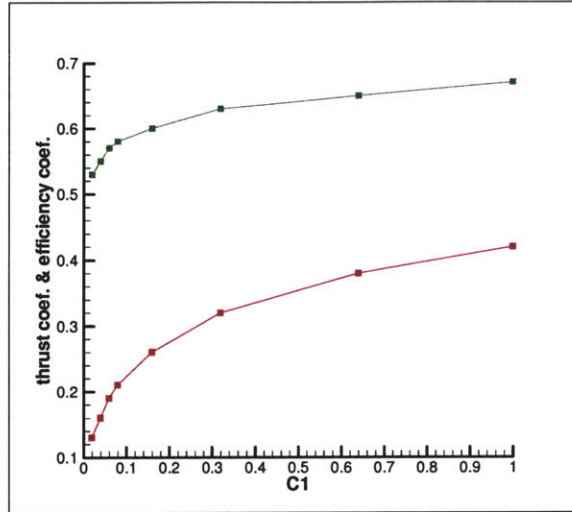
Figure 4-5: Dependent of thrust coefficient and efficiency on C_1. Red: thrust coefficient Green: efficiency. The parameters are: U=0.4 m/s, $S_t = 0.30$, $h_0/c = 0.75$, $\alpha_{max} = 10^o$, $\psi = 90^o$, $T/\triangle t = 32$.
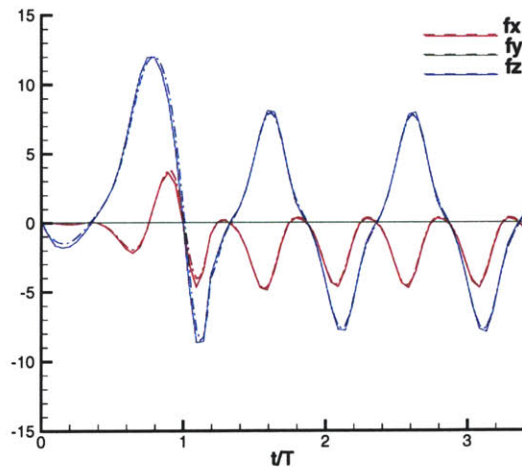
Figure 4-6: Illustration of convergence as the time step decreases by using linear distribution of the velocity potential on the first row of wake panels. Solid: $\frac{U\Delta t}{\Delta X_T} = 40$, Dashed: $\frac{U\Delta t}{\Delta X_T} = 30$, Dashed-dot: $\frac{U\Delta t}{\Delta X_T} = 20$. The parameters are: U=0.4 m/s, $S_t = 0.30$, $h_0/c = 0.75$, $\alpha_{max} = 10^o$, $\psi = 90^o$.

46

significant change in results if all wake panels were linearly distributed. This has been confirmed in our simulation. The details of the modification to use linear distribution of the singularities on the first row of the wake panels can be found in Hsin (1990).

4.3 Summary

In this chapter, we present the detailed low-order panel method used in our simulation. The discretization of the governing equation and the paneling of the foil surface are specified. The independence of the numerical results on the desingularization factors is discussed. In addition, A sinusoidal function is used to smooth the transition of an impulsively started foil, and the calculation of the fluid velocity on the foil surface and the unsteady pressure is introduced.

Furthermore, for the low-order boundary element method used for our simulation, we make an important modification. We remove the dependence of our numerical results on a free parameter which controls the length of the first row of the trailing-edge wake panels by using a linear distribution of the singularities on the first row of the trailing-edge wake panels following Hsin (1990).

Chapter 5

Leading-Edge Separation Model

We represent the leading-edge separation as a single thin shear layer in the same manner as its counterpart shed from the trailing edge. This model is supported by the flow visualizations in the experiments (Taneda 1977), which demonstrate that in the near field, the vortices are in the form of thin vortex sheets before individual vortices are generated through flow instability.

However, to implement our leading-edge separation model, first we need to determine the location of the leading-edge separation. Because of the finite curvature of the leading edge, which is different from the sharp trailing edge, the location for the leading-edge separation is extremely difficulty to predetermine, especially when the flow is unsteady because the separation location tends to move in unsteady flows (Taneda 1977). The second difficulty is that the leading-edge wake sheet goes into or through the foil body easily because of the Lagrange scheme of the wake relaxation in the boundary element simulation.

In this chapter, these two difficulties are addressed. In Section 5.1, the criteria for the location of the leading-edge separation are discussed. In Section 5.2, we present an algorithm to deal with the problem of the penetration of the wake into the body. This chapter is summarized in Section 5.3.

48

5.1 Location of Leading-Edge Separation

The separation position near the sharp trailing edge of the foil is always fixed at the tips. However, for the rounded leading edge the location where the leading-edge separation happens is not fixed. The position of the leading-edge separation is extremely difficult to predict, especially when the flow is unsteady. Furthermore, the position of the leading-edge separation tends to move in unsteady flows (Teneda 1977).

Because it is so difficult to predict the location of the leading-edge separation, one method to model the leading-edge separation is by a group of shear layers, each starting from a prescribed separation point (Zhu private communication 2004). However, this implementation yields two free parameters, which need to predetermined: (1) the size of the separation area, (2) the number of the separation lines. Because of this, the size of the separation area and the number of the separation lines have to be calibrated by experiments. Furthermore, the multiple leading-edge vortex sheets may interact with each other, which is problematic. In addition, the concept of multiple vortex sheets is not supported by experiments. In general, only one or two vortex sheets are shed from the rounded leading-edge (Teneda 1977).

A more pragmatic approach to address this issue is to consider a physical criterion to determine the location of the leading-edge separation.

5.1.1 Angle of Attack as Criterion for Separation Location

Minotti (2002) modeled the detachment of the leading vortex according to the angle of attack, or the angle between the velocity vector and the wing, in his unsteady two-dimensional theory. Angle of attack is used to decide on which side the detachment of the leading-edge vortex will happen (Minotti 2002). If the angle of attack is positive, then the detachment will happen on the lower side of the foil. If the angle of attack is negative, the detachment is on the upper side of the foil. This is rather simple implementation. Drawing on the limited success of Minotti (2002), we use this separation criterion. The location of the separation point is determined by the
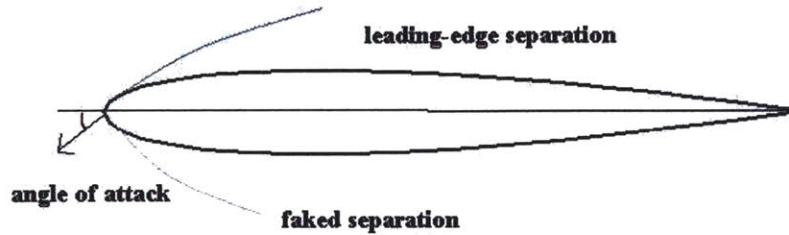
Figure 5-1: Illustration of the leading-edge separation and faked separation.

tangential point of the velocity of the leading edge at the maximum angle of attack to the foil surface.

In implementation, two wake sheets are shed from the specified separation location of each side of the foil near the leading edge. Each wake sheet is shed from the separation location tangential the direction of velocity at the maximum angle of attack. One wake sheet corresponds to the positive maximum angle of attack; the other corresponds to the negative maximum angle of attack. By the criterion of angle of attack, we determine which side of the wake sheet is included for the contribution of the leading-edge separation. For the wake sheet on the other side, where no leading-edge separation should happen, we exclude the contribution by setting the strength of the wake to zero. As Figure 5-1 shows, at each time step the wake sheet shed from only one side of the foil is included, while the wake sheet shed from the other side is called faked separation and its contribution is excluded. By this arrangement, only parts of each wake sheets contribute to the leading-edge separation. We can see the difference in the leading-edge wake sheet with and without the criterion of angle of attack from Figure 5-2. This is also illustrated in Figure 5-3, in which only the blue or red parts of each wake sheet are included, while the green parts are excluded by setting the strengths to zero.

The method above to account for the leading-edge separation will make our computation much easier to implement. Although this criterion is crude, The resulting forces compare well with those from experiments. The inclusion of the leading-edge separation improves the simulation results significantly.

However, this criterion does not account for the moving separation point. Thus

50
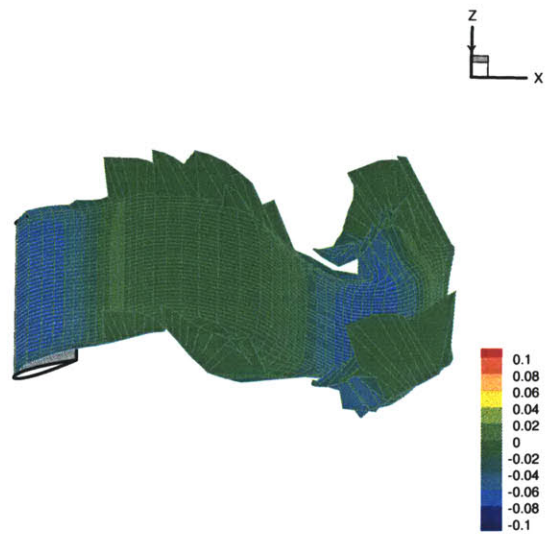
(a) Leading-edge wake sheet with the criterion of the angle of attack.
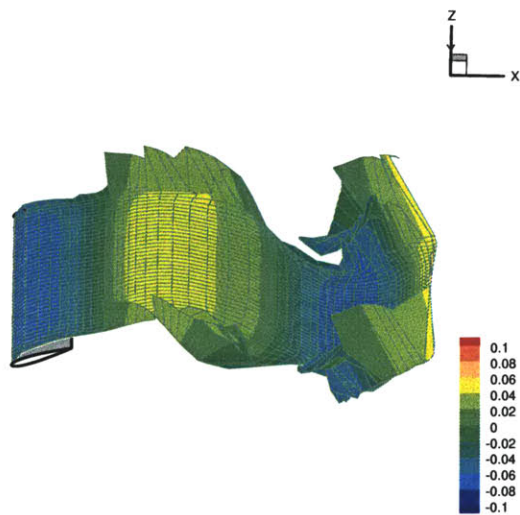
(b) Leading-edge wake sheet without the criterion of the angle of attack.

Figure 5-2: Comparison of the leading-edge wake sheet with and without the criterion of the angle of attack.
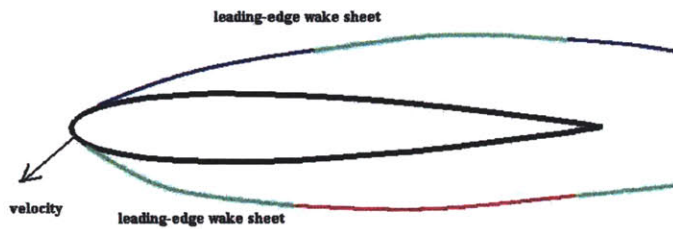
Figure 5-3: Illustration of the contribution of the leading-edge separation. Red and Blue: included in the contribution of the leading-edge separation, Green: excluded from the contribution of the leading-edge separation.

we are not satisfied with the tangential point as separation point. We can take a look at the Moore-Rott-Sears model that is more physical.

5.1.2 Moore-Rott-Sears model

The Moore-Rott-Sears model (Moore 1958; Rott 1956; Sears 1975 and Williams 1977) illustrates that the unsteady separation point is characterized by the simultaneous vanishing of the shear and the velocity at a point within the boundary layer as seen by an observer moving with the separation. This may serve as the separation criterion for our leading edge separation model. However, because of the potential flow assumption, the position of the separation point may be different from the prediction of boundary layer theory. Furthermore, the position of the vanishing of the shear and the position of the vanishing of the velocity in the reference frame of the moving separation are not the same as a result of potential flow assumption.

Our experiences in the simulation show that the position of the separation by the criterion of the vanishing of the velocity is around the leading edge, but not very near the leading edge. However, we have tried to simulate the heaving-pitching motion of the foil with a leading-edge wake from the separation location by this criterion, and found that the resulting forces differ little from those without leading-edge separation. Therefore, this separation criterion is not a good candidate for the prediction of the leading-edge separation in the boundary element simulation, with potential flow assumption.

52

### 5.1.3 Adverse Pressure Gradient as Criterion for Separation Location

This criterion states that in the adverse pressure region the flow separation happens. However, from the pressure distribution on the surface of the foil in Figure 5-4(b), we can see the region of the adverse pressure gradient is large. Figure 5-5 illustrates the large region of the adverse pressure gradient according to Figure 5-4(b). The adverse pressure gradient region starts from near the leading-edge and lasts to nearly the whole foil length.

Because of the large region of the adverse pressure gradient, it is difficult to determine the specific location of the leading-edge separation. Therefore, we tried to shed a number of wake sheets from the whole adverse pressure gradient region to approximate the leading edge separation. However, we could not obtain reasonable results. Using a number of wake sheets is also not physical, from what we observe in the experiments. In the experiments, only one or two shear layers are shed from the leading edge (Taneda 1977; Maresca et al. 1979; Ohmi et al. 1990 and 1991). From those experiments, we can also see the separation point is moving because of the unsteady motion.

After comparing the location of the tangential point with the starting point of the adverse pressure gradient, we find those two positions are almost or very near the same. Furthermore, the starting point of the adverse pressure gradient is also the position of the vanishing of the tangential force. Thus, the starting location of the adverse pressure gradients is a reasonable criterion for the position of the leading-edge separation, and this criterion is more physical. The separation of flow past a cylinder can serve as a good example. At high Reynolds numbers, the separation point of the laminar flow past a cylinder is near the starting point of the adverse pressure gradient. Therefore, we choose the starting points of the adverse pressure region or the local minimum of the pressure as the position of leading-edge separation, which satisfy
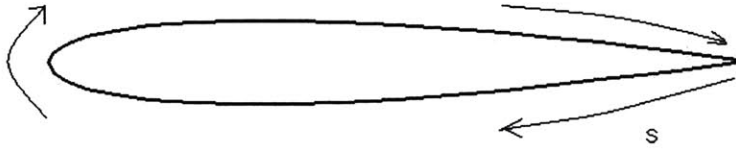
(a) Difinition of s: the arc length along the foil surface from the trailing edge. S is the total arc length.
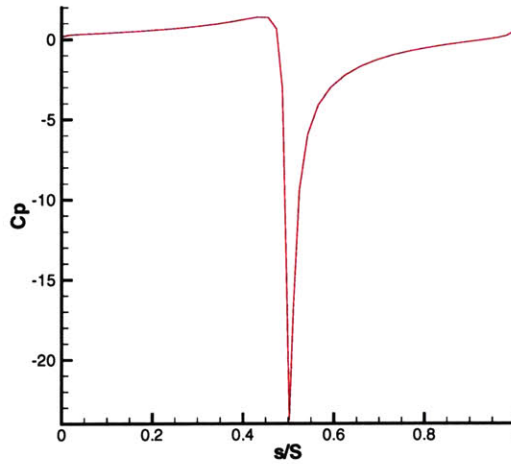
(b) Pressure distribution.

Figure 5-4: Pressure distribution along the surface of a foil. The parameters are: U=0.4 m/s, $S_t = 0.20$, $h_0/c = 0.75$, $\alpha_{max} = 30^o$, $\psi = 90^o$.
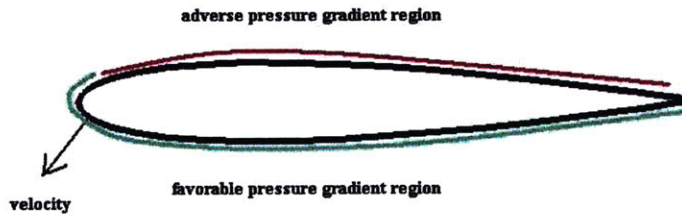

Figure 5-5: Adverse pressure region along the surface of a foil.

$$\frac{\partial^2 p}{\partial l^2}\Big|_{l_s} > 0 \tag{5.1}$$

and

$$\frac{\partial p}{\partial l}\Big|_{l_s} = 0 \tag{5.2}$$

where l_s is the separation point and l is defined from the leading edge to the tailing edge along the foil surface.

Figure 5-6 shows the strength of the wake sheets when shed from different locations: from the separation location we define, from the location ahead of the separation position we define, and from the location behind the separation position we define. We can see that the strength of the wake sheet is the largest when the wake sheet is shed from the separation location we define, which may support our criterion for the leading-edge separation.

By this separation criterion, we can see from Figure 5-7 that at one certain time step there is only one separation point near the leading edge, and it is at only one side of the foil. Therefore, only one wake sheet is shed from either the lower side or the upper side of the foil, as we see from the experiments. We note that in the half period when the angle of attack stays positive or negative, the separation point does not move. It only moves significantly after half a period, when the angle of attack changes its sign. This is because of the large curvature at the leading edge of the foil. The separation locations are highly localized near the leading edge, which agrees with the experiments (Taneda 1977). Over time, the leading-edge wake sheet is shed alternatively from the upper or lower side of the heaving-pitching foil, because of the movement of the separation points.

The drawback of using this criterion in our simulation is that the forces may not be smooth at the time when separation points move from one side of the foil to the other side. However, this limitation has only a negligible effect on the time average forces and efficiencies because at most times the forces are smooth.

55
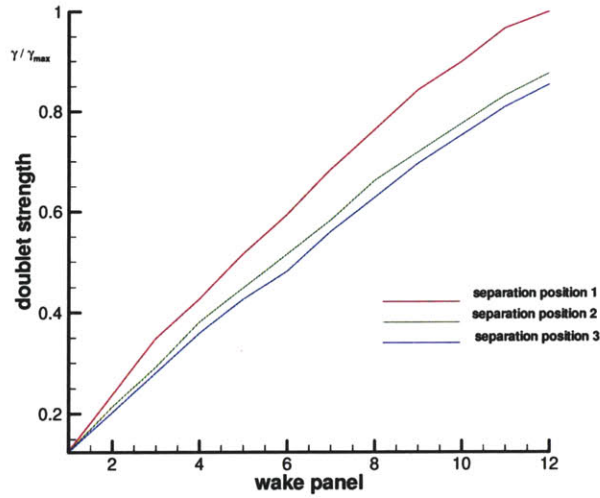
Figure 5-6: Doublet strength of the wake sheets shed from the different locations. Separation position 1: wake sheet shed from the separation location($\frac{\partial p}{\partial l} = 0$). Separation position 2: wake sheet shed from the location before the separation location we define. Separation position 3: wake sheet shed from the location behind the separation location we define.The parameters are: U=0.4 m/s, $S_t = 0.20$, $h_0/c = 0.75$, $\alpha_{max} = 30^o$, $\psi = 90^o$.

Figure 5-7: Movement of the position of the leading-edge separation (where $\frac{\partial p}{\partial l} = 0$) in one period. The minimum of each line is the separation point we define. Each line corresponds to one time step. Green: when angle of attack is positive. Red: when angle of attack is negative. The parameters are: U=0.4 m/s, $S_t = 0.20$, $h_0/c = 0.75$, $\alpha_{max} = 30^o$, $\psi = 90^o$.

56

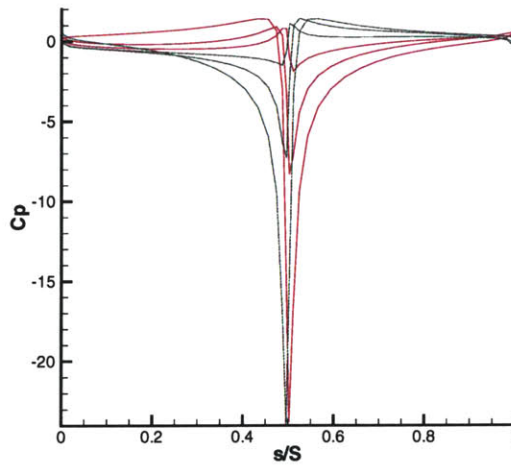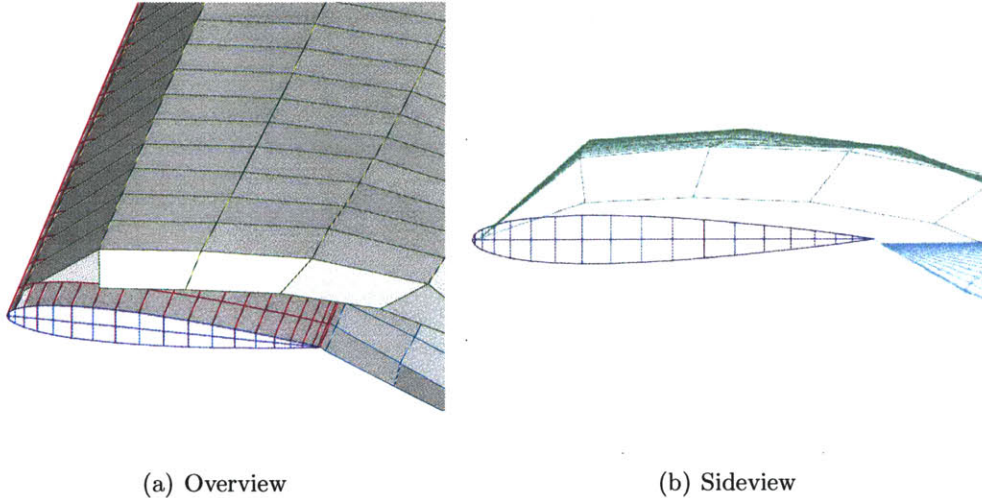(a) Overview (b) Sideview

Figure 5-8: Problem of wake penetration into the foil body.

5.2 Problem of Wake Penetration

The leading-edge wake will interact with the foil downstream. Thus, the study of the wake/body interference is of great importance in our leading-edge separation modeling. It is also important in vortex body interactions in the case of the body in the flow of incoming vortices (Donald *et al.* 1998), or the interactions between the upstream body and the downstream body (Yao and Liu 1998).

Because the panel method is a numerical method of Lagrange description of the flow field, the vortex wake sheet may not always circumvent the body and it can easily go into or go through the thin foil when the common wake relaxation technique is used. Figure 5-8 shows the wake penetration into the body. It is difficult to deal with the penetration of the wake into the heaving-pitching body because the flow is unsteady. Another difficulty is that when the wake goes very near the body, the induced velocity at any point between the surface panel and wake panel is un-physically high. Within a small time step, the fluid particle will travel a long distance. The induced velocity may approach infinity at the edges of the surface panels in most high order panel methods (Terzi and Chiu 1997).

To solve the problem of the penetration of the wake into the foil, in the preliminary work of Zhu (private communication 2004), the wake was allowed to go into the body

57

freely and a very large desingularization factor was used for the numerical difficulty when part of the wake is in the body. The desingularization factor in his simulation is the order of the foil length. However, as a result of the large desingularization factor, the set of the linear equations is not solved accurately because the influence coefficients in the set of linear equations are changed greatly by the large desingularization factor. Therefore, he obtained a much weaker leading-edge separation in his simulation. Furthermore, by the large desingularization factor the leading-edge wake sheets are essentially far away from the foil.

Chen and Williams (1987) simply deleted the segment inside the thin foil if the wake sheets went into or through the body. Although it is not physical, we tried this method because it is simplest to implement. However, we find that the error by this method is unpredictable. Sometimes the resulting forces are larger than those of experiments and sometimes smaller.

5.2.1 Push-out Method

Another method to deal with the wake penetration problem is the push-out model used by Wolfgang (1999). It is relatively simple model incorporating some physics. In this model, the location of the wake after convection is cross referenced and any panels which may have penetrated the body are repositioned outside the body panel close to where the wake had been convected.

Similarly, in our simulation, when the wake sheet goes into the body or goes through the body, it will be pushed outside the nearest body panel from which it comes and in this way the wake sheet is kept at one side of the foil. For a preliminary try, one constant value is used in the calculation of the distance between the foil surface and wake corner point which is pushed out. However, the resulting forces from the push-out model are not smooth, as shown in Figure 5-9.
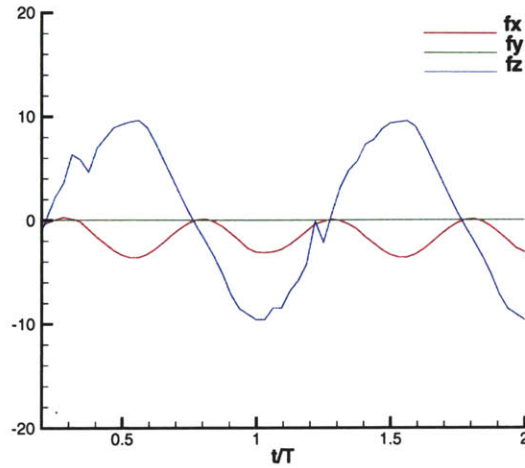
58

Figure 5-9: Resulting forces are not smooth by the push-out method. The parameters are: U=0.4 m/s, $S_t = 0.20$, α_{max}=30°, h_0/c=0.75, $\psi = 90°$.

5.2.2 Pre-check Method

The push-out method restricts the complexity of the wake body interaction. In our simulation, the wake which interacts with the body is shed from the leading edge and thus the wake body interaction is important to study the effect of leading-edge separation. To this end, we use the pre-check technique which includes the following steps:

- 1. Calculate the foil position at the next time step

- 2. Calculate the wake sheet position at the next time step.

- 3. Compare the wake sheet position and foil position at the next time step to see if the wake is very near the foil or if the wake goes into or through the foil.

- 4. If the wake is very near the foil or if the wake goes into or through the foil at the next time step, then go back to the current time step.

- 5. At the current time step, change the normal velocity of the wake into the normal velocity of the nearest foil panel so that at the next time step, the wake will not penetrate the foil.

This method is a simple version of the close approach method (Terzi and Chiu 1997). Similar method is also used by Yao and Liu (1998) in their blade-blade interaction problem, in which one downstream blade is in the wake field of the other upstream blade. Because it is first-order method, the resulting forces are smooth.

In our simulation, a small distance s_ϵ, by which the wake too near the foil, is defined. When the distance from the wake panel corner point to the nearest foil panel d is less than s_ϵ ($d < s_\epsilon$), then the wake is too near the foil and the modification of the velocity of the wake corner point will be made. We find that the simulation results are not sensitive to this small distance as long as it is small enough. The small distance s_ϵ in our simulation is chosen as one tenth of the foil thickness b_{thick} ($s_\epsilon = \frac{1}{10} b_{thick}$).

By this pre-check technique that we use to enforce no penetration free-slip boundary condition, the vortices will remain attached near the free-slip solid boundary if this boundary is a flat surface. Because of the potential flow theory, the vortices will not rebound because of the free ship boundary condition. Therefore, the technique is reasonable in the simulation with potential flow assumption. However, the phenomenon of rebound of the vortices occurs on the boundary of either no slip or stress-free. The rebound is explained by viscous effects (Peace 1983; Barker 1977 and Doligalski 1994).

5.3 Summary

We model the leading-edge separation as a single thin shear layer in the same manner as its counterpart shed from the trailing edge. This model is supported by the flow visualizations in the experiments (Taneda 1977), which demonstrate that in the near field, the vortices are in the form of thin vortex sheets before individual vortices are generated through flow instability. However, for the rounded leading edge the location where the leading-edge separation happens is variable. The position of the leading-edge separation is extremely difficult to predict, especially when the flow is unsteady. Furthermore, the position of the leading-edge separation tends to move in the unsteady flows (Teneda 1977).

To predict the separation location near the leading-edge, several criteria for the separation location are discussed. We found that the most promising criterion to be the starting points of the adverse pressure gradient as the location of leading-edge separation, which satisfy

$$\frac{\partial^2 p}{\partial l^2}\Big|_{l_s} > 0 \tag{5.3}$$

and

$$\frac{\partial p}{\partial l}\Big|_{l_s} = 0 \tag{5.4}$$

where l_s is the separation point and l is defined from the leading edge to the tailing edge along the foil surface.

In implementation, the separation location is determined in the simulation without leading-edge separation. Next, with the predetermined separation location near the leading-edge, we simulate the heaving-pitching foil with a constant straight forward speed. Because the separation location is decided at each time step, the moving separation location can be accounted for.

Because the leading-edge wake sheet is shed by the Lagrange scheme of wake relaxation in the boundary element simulation, the leading-edge wake sheet goes into or through the thin foil easily. We present a pre-check algorithm to deal with the penetration of the leading-edge wake into the foil body.

Chapter 6

Performance of Leading-Edge Separation Model

We apply our leading-edge separation model in our modified low-order boundary element method to examine the thrust and propulsion efficiency of a NACA0012 foil undergoing heave and pitch motions. The adverse pressure gradient criterion and the pre-check technique are used in our leading-edge separation model. Validation of our leading-edge separation model is conducted by convergence tests. The simulation results are compared with those from experiments (Read 2000).

This chapter is organized in the following way. In Section 6.1 and Section 6.2, we summarize our leading-edge separation model and the numerical method that we used, respectively. We validate our numerical simulation by the convergence tests in Section 6.3. The sensitivity tests of the numerical parameters are presented in Section 6.4. In Section 6.5, the strength of the leading-edge separation is discussed. In Section 6.6, the performance of our leading-edge separation model is discussed by comparing our numerical results with the experimental measurements by Read (2000) on the dynamics of heaving-pitching foils. The main conclusion from our simulation results is summarized in Section 6.7.

6.1   Summary of Leading-Edge Separation Model

We model the leading-edge separation as a single thin shear layer in the same manner as its counterpart shed from the trailing-edge. This model is supported by the flow visualizations in the experiments (Taneda 1977), which demonstrate that in the near field, the vortices are in the form of thin vortex sheets before individual vortices are generated through flow instability. However, for the rounded leading edge the location where the leading-edge separation happens is variable. The position of the leading-edge separation is extremely difficult to predict, especially when the flow is unsteady. Furthermore, the position of the leading-edge separation tends to move in the unsteady flows (Teneda 1977). To predict the separation location near the leading edge, we use the criterion of the starting points of the adverse pressure gradient as the location of leading-edge separation, which satisfy

$$\frac{\partial^2 p}{\partial l^2}\Big|_{l_s} > 0 \qquad\qquad (6.1)$$

and

$$\frac{\partial p}{\partial l}\Big|_{l_s} = 0 \qquad\qquad (6.2)$$

where l_s is the separation point and l is defined from the leading edge to the tailing edge along the foil surface.

This criterion is physical and can account for the moving separation points in unsteady flows. In implementation, the separation location is determined in the simulation without leading-edge separation. Next, with the predetermined separation location near the leading-edge, we simulate the heaving-pitching foil with a constant straight forward speed. Because the separation location is decided at each time step, the moving separation location can be accounted for.

Although we simulate a two-dimensional motion of the three-dimensional foil with our leading-edge separation model, the application of our leading-edge separation model can be easily extended to the simulation of the three-dimensional motions of a three-dimensional foil.

Because the leading-edge wake sheet is shed by the Lagrange scheme of wake relaxation in the boundary element simulation, the leading-edge wake sheet goes into or through the thin foil easily. We present a pre-check algorithm to deal with the penetration of the leading-edge wake into the foil body. The pre-check algorithm includes the following steps:

- 1. Calculate the foil position at the next time step

- 2. Calculate the wake sheet position at the next time step.

- 3. Compare the wake sheet position and foil position at the next time step to see if the wake is very near the foil or if the wake goes into or through the foil.

- 4. If the wake is very near the foil or if the wake goes into or through the foil at the next time step, then go back to the current time step.

- 5. At the current time step, change the normal velocity of the wake into the normal velocity of the nearest foil panel so that at the next time step, the wake will not penetrate the foil.

6.2   Summary of Numerical Method

Following Zhu *et al.* (2002), we solve the governing equations with the boundary conditions by a low order panel method in order to obtain the body influence potential ϕ_b. In this approach, both the body surface S_b and the wake sheets S_w are discretized into finite numbers of quadruple panels (Katz 1991). Over each panel the singularities are distributed with constant strengths at the collocation points. To increase the accuracy of prediction of the unsteady flow field, smaller panels are used in the regions of presumed rapid potential variation, such as the regions of the large curvature of the foil.

At any time t, the set of discretized linear equations of the body influence potential $\Phi_b(\mathbf{x}_i, t)$ ($i = 1, ..., N_b$, where N_b is the total number of body surface panels) at each

panel collocation point are

$$-2\pi\Phi_b(\mathbf{x}_i,t) + \sum_{j=1,j\neq i}^{N_b}(\Phi_b(\mathbf{x}_j,t)C_{ij}) + \sum_{k=1}^{N_w}(\Phi_w(\mathbf{x}_k,t)C_{ik}) = \sum_{j=1}^{N_b}(\frac{\partial\Phi_b(\mathbf{x}_j,t)}{\partial n}B_{ij}) \quad (6.3)$$

where N_b is the total number of the body surface panels, N_w is the total number of the wake panels. C_{ij}, C_{ik}, B_{ij} are body influence coefficients, wake influence coefficients and the normal velocity influence coefficients for the velocity potential, respectively.

$$C_{ij} = \int\int_{S_b}\frac{\partial 1/r_{ij}}{\partial n}dS \qquad (6.4)$$

$$C_{ik} = \int\int_{S_w}\frac{\partial 1/r_{ik}}{\partial n}dS \qquad (6.5)$$

$$B_{ij} = \int\int_{S_b}\frac{1}{r_{ij}}dS \qquad (6.6)$$

where $r_{ij} = |\mathbf{x}_i - \mathbf{x}_j|$, $r_{ik} = |\mathbf{x}_i - \mathbf{x}_k|$.

The right side of Equation (6.3) is known by applying the kinematic boundary condition below for each panel on the body surface.

$$\frac{\partial\Phi_b(\mathbf{x}_i,t)}{\partial n} = \mathbf{V}_b(\mathbf{x}_i,t)\cdot\mathbf{n} \qquad (6.7)$$

where $\mathbf{V}_b(\mathbf{x}_i,t)$ is the prescribed body motion on each panel and $\mathbf{n}$ is the unit normal vector of the body surface pointing into the body.

$\Phi_w(\mathbf{x}_k,t)$ is known except at the first row of the wake panels, from the previous time step by the time-stepping wake model. $\Phi_w(\mathbf{x}_k,t)$ for the first row of the wake panels, is related to $\Phi_b(\mathbf{x}_i,t)$ through Kutta condition. Thus, the unknowns are only $\Phi_b(\mathbf{x}_i,t)$.

At each time step, this set of linear equations is solved with the Kutta condition to obtain the body velocity potential $\Phi_b(\mathbf{x}_i,t)$. Then the unknown strengths for the first row of the wake panels can be obtained by the Kutta condition and after that, the wake is updated and convected downstream with the local flow velocities. Therefore, $\Phi_b(\mathbf{x}_i,t)$ and $\Phi_w(\mathbf{x}_k,t)$ can be obtained by the iterative scheme. After that, the flow field at the time step t can be determined by the body influence potential $\Phi_b(\mathbf{x},t)$

and the wake influence potential $\Phi_w(\mathbf{x}, t)$.

For the low-order boundary element method used for our simulation, we also made an important modification. We removed the dependence of our numerical results on a free parameter C_1, which controls the length of the first row of the trailing-edge wake panels, by using a linear distribution of the singularities on the first row of the trailing-edge wake panels, following Hsin (1990). Thus in our current simulation, we use the linear distribution of singularities for the first row of the trailing-edge wake panels and use the constant distribution of singularities for all other panels.

6.3 Validation by Convergence Tests

The validation of the low-order boundary element method has been examined extensively in previous work (Zhu *et al.* 2002). Further it is also examined in Chapter 4 in this thesis and necessary modification is made. In the present investigation, we will only investigate the convergence of our numerical algorithm with our leading-edge separation model, which is novel.

First we examine the convergence with the time step decreasing. From Figure 6-1, we can see the resulting forces converge as the time step decreases. The convergence can also be seen from Table 6.1 as we reduce the time step. Next, as the panel size decreases, we can see the convergence from Figure 6-2 and Table 6.2. When the panel size changes, the exact location for the leading-edge separation may be slightly different. Thus, the convergence for decreasing the panel size is slower than that for decreasing the time step. The parameters of the case used for the convergence tests are Forward speed U=0.4 m/s, Strouhal number $S_t = 0.2$, maximum angle of attack= 30°, heave chord ratio $h_0/c = 0.75$, and phase angle between heave and pitch $\psi = 90^o$.

From Figure 6-1 and 6-2, we can see the thrust coefficients are asymmetric. The peak thrust coefficient value for the upstroke is different from that of the downstroke. The similar asymmetric thrust coefficients were also found in the experiments (Prempraneerach *et al.*, 2003). Lewin and Haj-hariri (2003) discussed the asymmetry in mid- and high-frequency range in their simulation of a two-dimensional heaving air-
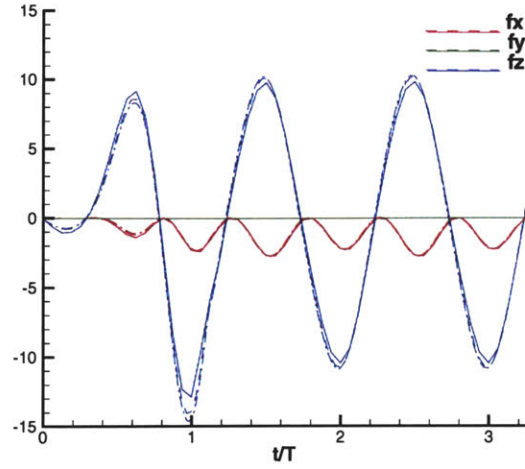
Figure 6-1: Convergence by decreasing time step. Solid: Δt, Dashed: $\Delta t/2$, Dashed-Dot: $\Delta t/4$, where $\Delta t = \frac{T}{16}$. The parameters are: U=0.4 m/s, $S_t = 0.20$, $h_0/c = 0.75$, $\alpha_{max} = 30^o$, $\psi = 90^o$.

$\frac{T}{\Delta t}$	8	16	32	64
C_t	0.260	0.228	0.223	0.221

Table 6.1: Convergence of the mean thrust coefficient C_t with respect to the time step Δt. The parameters are: U=0.4 m/s, $S_t = 0.20$, $h_0/c = 0.75$, $\alpha_{max} = 30^o$, $\psi = 90^o$. 40*40 panels on the foil surface are used.

foil in a viscous flow. The asymmetric thrust coefficients result from the asymmetric wake field.

Number of panels	30*30	40*40	50*50
C_t	0.209	0.223	0.235

Table 6.2: Convergence of the mean thrust coefficient C_t with respect to the number of the panels on the foil surface. The parameters are: U=0.4 m/s, $S_t = 0.20$, $h_0/c = 0.75$, $\alpha_{max} = 30^o$, $\psi = 90^o$. The time step is $T/\Delta t$.

67
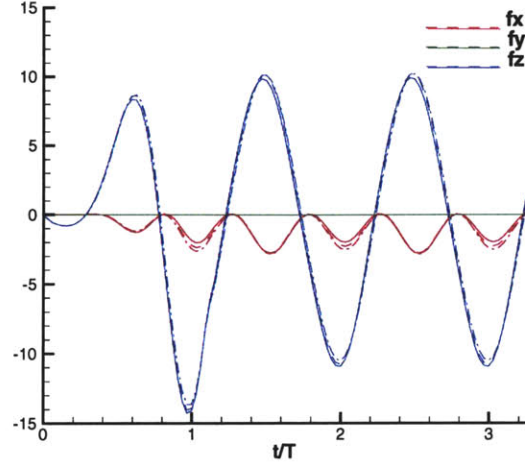
Figure 6-2: Convergence by decreasing panel size. Solid: 30*30 panels, Dashed: 40*40 panels, Dashed-dot: 50*50 panels. The parameters are: U=0.4 m/s, $S_t = 0.20$, $h_0/c = 0.75$, $\alpha_{max} = 30^o$, $\psi = 90^o$.

6.4 Discussion of Numerical Parameters

The parameters used in our numerical simulation with our leading-edge separation model are the two desingularization factors (wake desingularization factor δ_w and body desingularization factor δ_s) and the small distance s_ϵ by which the wake too near the foil is defined.

Independence of the simulation results on the two desingularization factors is discussed in Chapter 4. The sensitivity of the numerical results with respect to those two desingularization factors are investigated as shown in Table 6.3. We can see for a large range of the two desingularization factors that the variation of the results is very small (less than 0.001%). The case for the sensitivity tests is the same as that for the convergence tests.

The simulation results are also not sensitive to this small distance s_ϵ as long as it is small enough. The small distance s_ϵ in our simulation is chosen as one-tenth of the foil thickness b_{thick} ($s_\epsilon = \frac{1}{10}b_{thick}$).

68

$\frac{\delta_s}{c} / \frac{\delta_w}{c}$	0.005	0.001	0.0005	0.0001
0.005	0.223001	0.222999	0.222999	0.222999
0.001	0.222999	0.223000	0.223000	0.223000
0.0005	0.222999	0.223000	0.223000	0.223000
0.0001	0.222999	0.223000	0.223000	0.223000

Table 6.3: Sensitivity of mean thrust force coefficient C_t on a heaving-pitching foil with a constant straight forward speed U with respect to the wake desingularization δ_w and the body desingularization factor δ_s. The parameters are: U=0.4 m/s, $S_t = 0.20$, $h_0/c = 0.75$, $\alpha_{max} = 30^o$, $\psi = 90^o$. 40*40 panels on the foil surface are used and the time step is $T/\triangle t$.

6.5   Strength of Leading-Edge Separation

The leading-edge wake sheet is obtained in the same manner as its counterpart at the trailing-edge. The strength of the leading-edge separation is solved by using the Kutta condition at the leading edge in the same way as that of the trailing-edge separation. From Figure 6-3, we can see that the strength of the leading-edge wake sheet is of the same order of magnitude as that of the trailing-edge wake. This agrees with the findings that the leading-edge separation is significant in the structure of the wake within a large range of parameters ($0.3 < S_t < 0.5$ and $13^o < \alpha_{max} < 36^o$) (Anderson *et al.* 1998)

6.6   Performance of Leading-Edge Separation Model

We apply the boundary element method, together with our model to simulate the leading-edge separation, to examine the hydrodynamic performance of an oscillating foil. We simulate the same heaving-pitching motions of an oscillating foil at different Strouhal numbers and maximum angles of attack as carried out by Read (2000) in the experiments. Our simulation results are compared with those of the experiments (Read 2000) to demonstrate the validity and accuracy of our leading-edge separation model.

We consider the heaving-pitching motion of the foil with two different heaving amplitudes, $h_0/c = 0.75$ and $h_0/c = 0.10$. The simulations are conducted with and
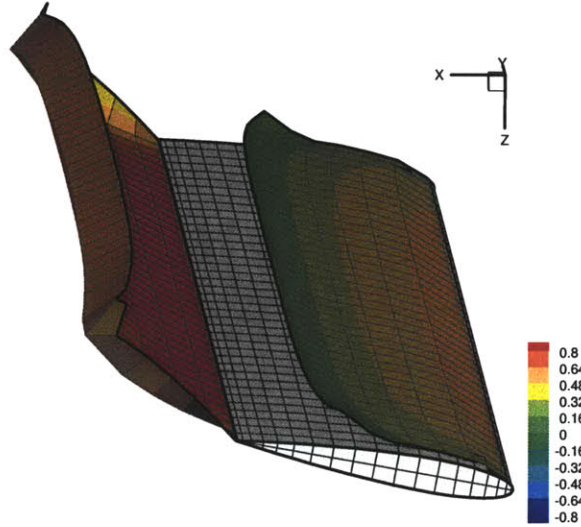
Figure 6-3: Comparison of the strengths of the leading-edge separation and the trailing-edge separation. The parameters are: $U = 0.4m/s$, $S_t = 0.30$, $\alpha_{max} = 30^o$, $h_0/c = 0.75$, $\psi = 90^o$.

without the leading-edge separation in the parameter range of $S_t \in (0.2, 0.4)$ and $\alpha_{max} \in (15^o, 40^o)$. The contribution from the leading-edge vortices is illustrated by the discrepancy between the two results.

6.6.1 Simulation Results for $h_0/c = 0.75$

Our simulation results for $h_0/c = 0.75$ are compared with those of the experiments (Read 2000). First we compare the thrust coefficient and propulsion efficiency as functions of the Strouhal numbers at different maximum angles of attack. Then the thrust coefficient and propulsion efficiency as functions of the maximum angles of attack are compared at different Strouhal numbers. After that, a summary of our comparison is presented.

Dependence of Simulation Results on Strouhal Numbers at Different Maximum Angles of Attack

Figure 6-4 shows the mean thrust coefficient C_t and the mean propulsion efficiency η as functions of the Strouhal number at a relatively small maximum angle of attack

($\alpha_{max} = 15^o$). We can see that at small Strouhal numbers the resulting thrust co-efficient and propulsion efficiency without the leading-edge separation compare well with those of the experiments and the inclusion of the leading-edge vortices does not improve the prediction of the thrust coefficient and propulsion efficiency. However, at large Strouhal numbers, the numerical model with the leading-edge separation gives a better prediction. This could be explained by the fact that at small Strouhal numbers the numerically imposed leading-edge separation may un-physically enforce the vortex separation near the leading edge.

If we increase the maximum angle of attack to $\alpha_{max} = 20^o$, we can see from Figure 6-5 that without the leading-edge separation, the numerical model over-predicts both the mean thrust coefficient and the propulsion efficiency. The discrepancy in efficiency is especially large and it is larger than 40%. However, the inclusion of the leading-edge separation effects reduces the discrepancy. The results with the leading-edge separation compare remarkably well with those from the experiments. The simulation results are within an error of less than 10% from the experimental measurements. As the Strouhal number S_t increases, the prediction of the thrust coefficient becomes better. This can be explained as follows. When S_t increases, the frequency of the heaving-pitching motion increases as we fix the heave amplitude and the forward speed. At higher frequencies, the interaction between the leading-edge wake and foil body becomes more important.

At maximum angle of attack $\alpha_{max} = 25^o$, from Figure 6-6 we can draw similar conclusions. The prediction with the leading-edge separation is much better than that without the leading-edge separation. The results without the leading-edge separation model have a larger discrepancy from those of the experiments at larger maximum angles of attack. The resulting thrust coefficient and the propulsion efficiency with our leading-edge separation model compare well with the results from the experiments.

Figure 6-7 shows the mean thrust coefficient and the propulsion efficiency at the maximum angle of attack $\alpha_{max} = 30^o$. Although we can still see the discrepancy between the simulation results with the leading-edge separation and those of the experiments at small Strouhal numbers, the prediction with the leading-edge separation
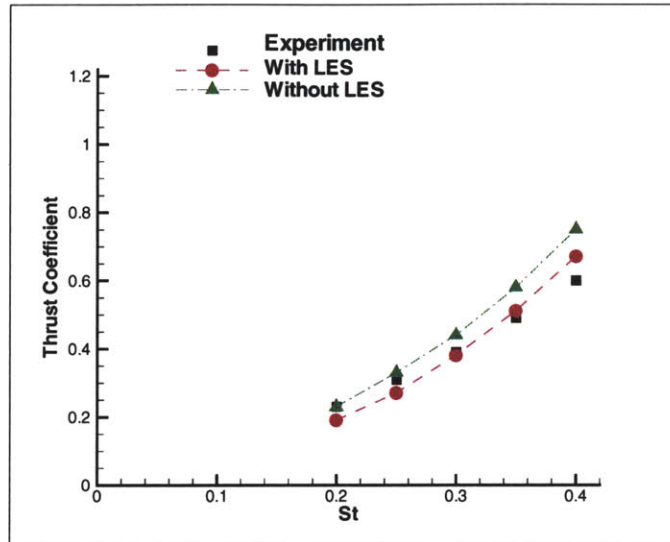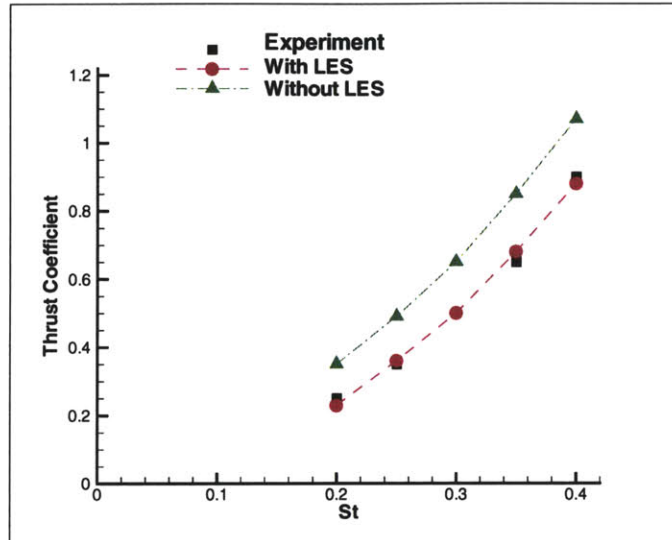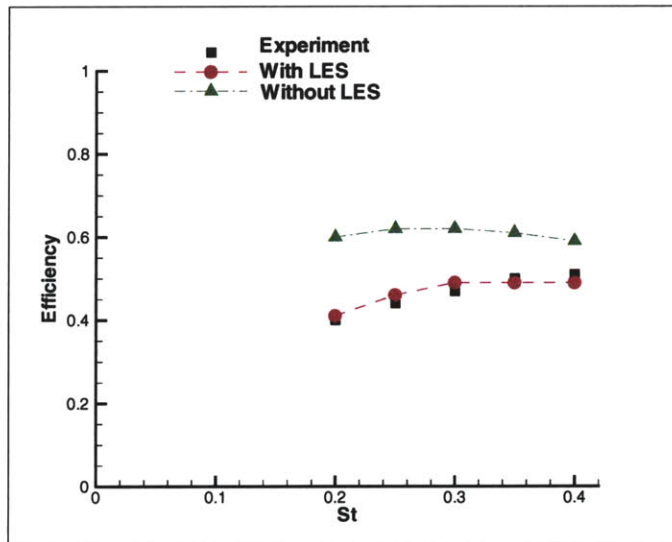
(a) Mean thrust coefficient
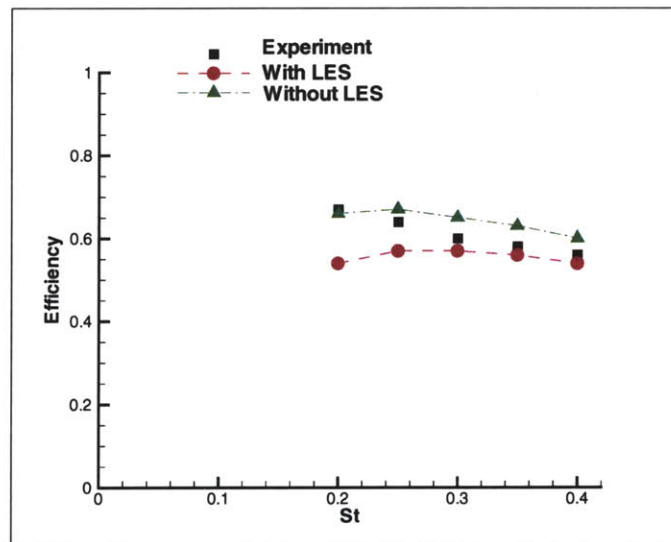
(b) Mean efficiency

Figure 6-4: Maximum angle of attack $\alpha_{max} = 15^o$.
Mean thrust coefficient and mean efficiency of a heaving-pitching foil with heave chord ratio $h_0/c = 0.75$ and phase angle between heave and pitch $\psi = 90^o$.

is much better than that without the leading-edge separation.

As the maximum angle of attack is further increased, we can see the discrepancy between the numerical results with our leading-edge separation model and the experimental results at the whole range of Strouhal numbers in Figure 6-8 and Figure 6-9. However, as compared with the results without the leading-edge separation, the prediction by our leading-edge separation model is much improved.

To summarize, our numerical results with leading-edge separation compare remarkably well with those of the experiments especially at the maximum angles of attack for $30^o > \alpha_{max} > 15^o$. However, there is still discrepancy between the numerical results and those of the experiments for $\alpha_{max} > 30^o$, although the prediction with leading-edge separation is much improved compared with that without leading-edge separation.

Dependence of Simulation Results on Maximum Angles of Attack at Different Strouhal Numbers

Figure 6-10 and 6-11 show the mean thrust coefficient C_t and the mean propulsion efficiency η as functions of the maximum angles of attack at relatively small Strouhal numbers ($S_t = 0.2$ and $S_t = 0.25$). We can see that at small Strouhal numbers the thrust coefficient and propulsion efficiency are over-predicted in the whole range of the maximum angle of attack without the inclusion of the leading-edge separation. The resulting thrust coefficient and propulsion efficiency with the leading-edge separation compare well with those of the experiments (Read 2000) at relatively small maximum angles of attack ($15^o < \alpha_{max} < 25^o$). At large maximum angles of attack, the discrepancy between the simulation results with the leading-edge separation and the experimental results (Read 2000) is obvious. However, the simulation results with the leading-edge separation are much improved as compared with those without the leading-edge separation. In addition, our simulation with the leading-edge separation capture the correct trend of the thrust coefficients, first increase with the maximum angles of attack at lower maximum angles of attack and then decrease at higher maximum angles of attack.
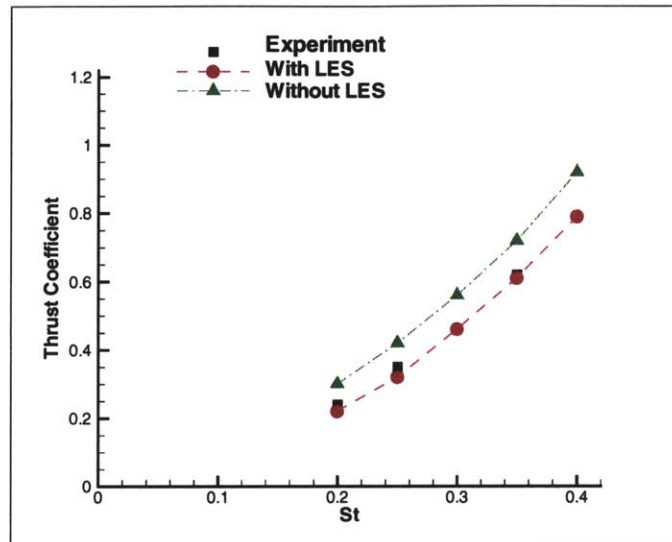
(a) Mean thrust coefficient
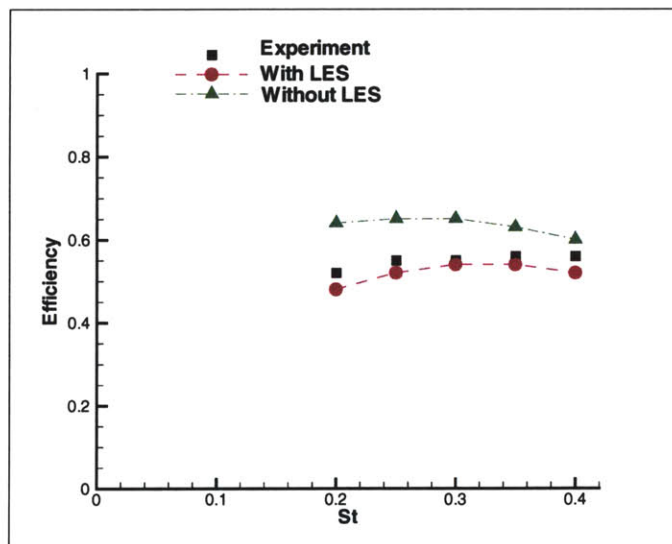
(b) Mean efficiency

Figure 6-5: Maximum angle of attack $\alpha_{max} = 20^o$.
Mean thrust coefficient and mean efficiency of a heaving-pitching foil with heave chord ratio $h_0/c = 0.75$ and phase angle between heave and pitch $\psi = 90^o$.
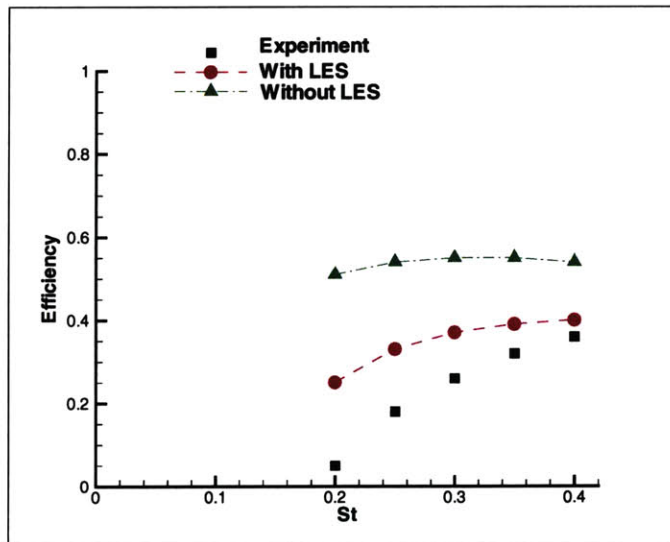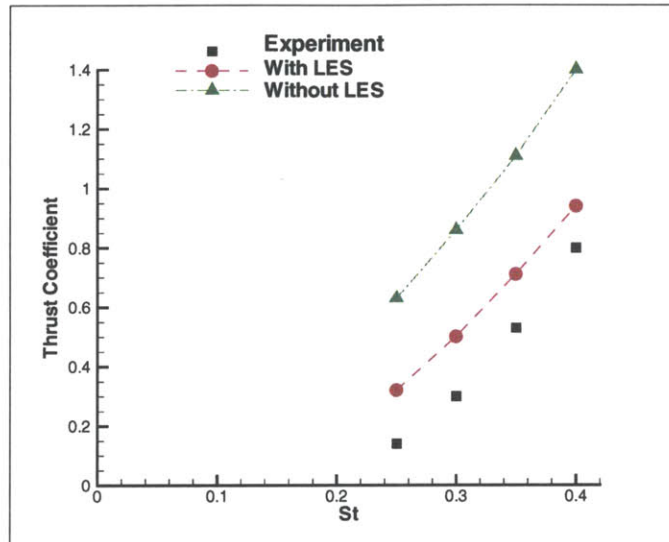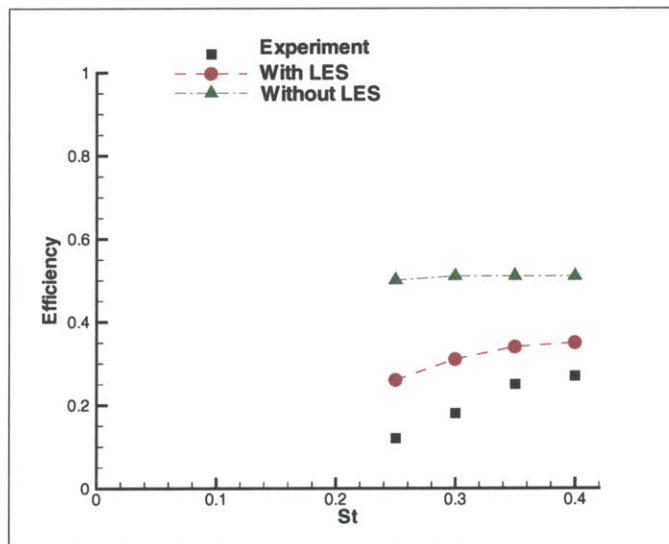
(a) Mean thrust coefficient

(b) Mean efficiency

Figure 6-6: Maximum angle of attack $\alpha_{max} = 25^o$.
Mean thrust coefficient and mean efficiency of a heaving-pitching foil with heave chord ratio $h_0/c = 0.75$ and phase angle between heave and pitch $\psi = 90^o$.

75
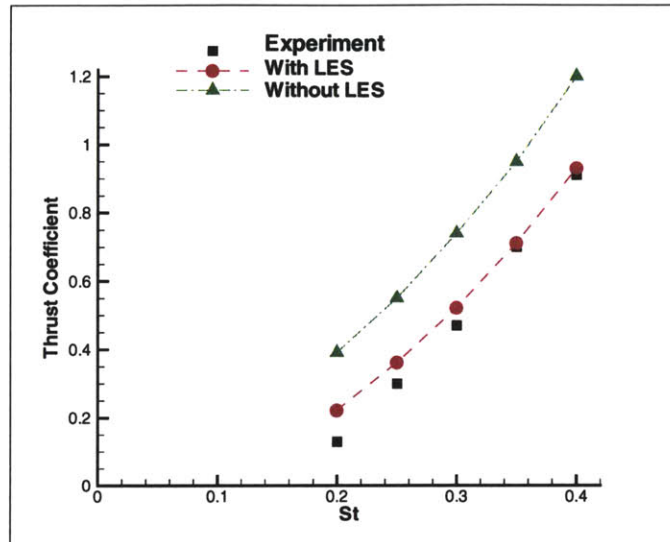
(a) Mean thrust coefficient
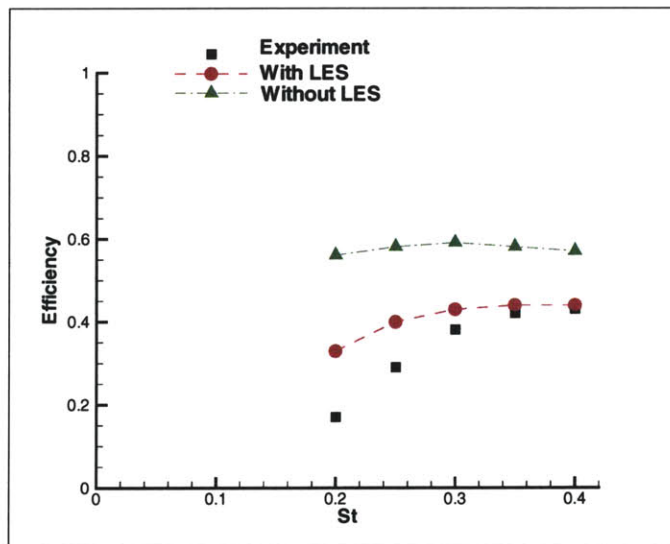
(b) Mean efficiency

Figure 6-7: Maximum angle of attack $\alpha_{max} = 30^o$.
Mean thrust coefficient and mean efficiency of a heaving-pitching foil with heave chord ratio $h_0/c = 0.75$ and phase angle between heave and pitch $\psi = 90^o$.

76
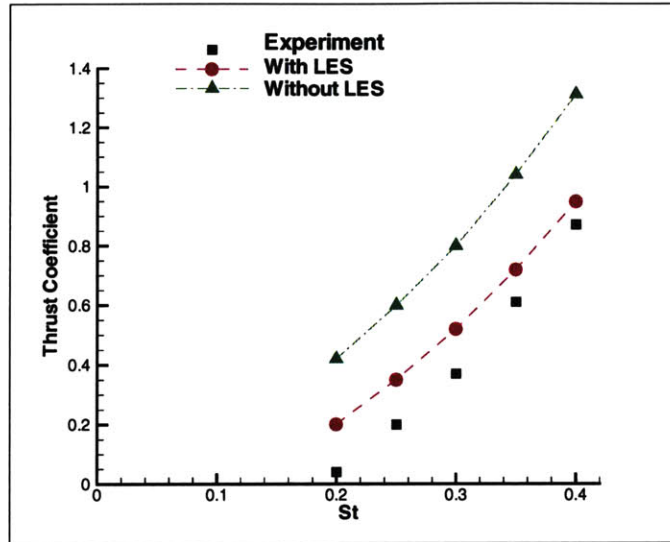
(a) Mean thrust coefficient

(b) Mean efficiency

Figure 6-8: Maximum angle of attack $\alpha_{max} = 35^o$.
Mean thrust coefficient and mean efficiency of a heaving-pitching foil with heave chord ratio $h_0/c = 0.75$ and phase angle between heave and pitch $\psi = 90^o$.

(a) Mean thrust coefficient

(b) Mean efficiency

Figure 6-9: Maximum angle of attack $\alpha_{max} = 40^o$.
Mean thrust coefficient and mean efficiency of a heaving-pitching foil with heave chord ratio $h_0/c = 0.75$ and phase angle between heave and pitch $\psi = 90^o$.

At $S_t = 0.3$, $S_t = 0.35$ and $S_t = 0.4$, we can see that our simulation results with the leading-edge separation compare well with those of the experiments at the maximum angles of attack of $15^o < \alpha_{max} < 30^o$ from Figure 6-12 to Figure 6-14. As the Strouhal number increases, the discrepancy between the simulation results with the leading-edge separation and the experimental results (Read 2000) becomes smaller at high maximum angles of attack ($\alpha > 30^o$).

In conclusion, the performance of our simulation with the leading-edge separation become better as the Strouhal number increases.

Summary of Simulation Results

Our numerical results compare remarkably well with those of the experiments especially at the maximum angles of attack of $15^o < \alpha_{max} < 30^o$. Although there is still discrepancy between the numerical results and those of the experiments for $\alpha_{max} > 30^o$, the prediction with leading-edge separation is much improved compared with that without leading-edge separation. As the Strouhal number increases, the performance of our simulation with the leading-edge separation becomes better.

Figure 6-15 summarizes the variation of the mean thrust coefficient C_t when the Strouhal number S_t is within the range $S_t \in (0.2, 0.4)$ and the maximum angle of attack $\alpha_{max} \in (15^o, 40^o)$. Figure 6-16 summarizes the variation of the mean propulsion efficiency in the same range of the Strouhal numbers and maximum angles of attack. From those figures, we can see that the overall performance of the numerical simulation with our leading-edge separation model is much better as compared with that without the leading-edge separation.

The prediction with the leading-edge separation is much better than that without the leading-edge separation as the maximum angle of attack increases in the range of $15^o < \alpha_{max} < 25^o$. This can be explained by the fact that the leading-edge separation may not happen or is very weak for the lower maximum angles of attack. By the criterion of leading-edge separation (Tuck 1991) that angle of attack should be greater than $0.818(r/c)^{1/2}$ for an airfoil of chord c and finite nose radius of curvature r, we find that the angle of attack must be greater than 18.7^o for the leading-edge
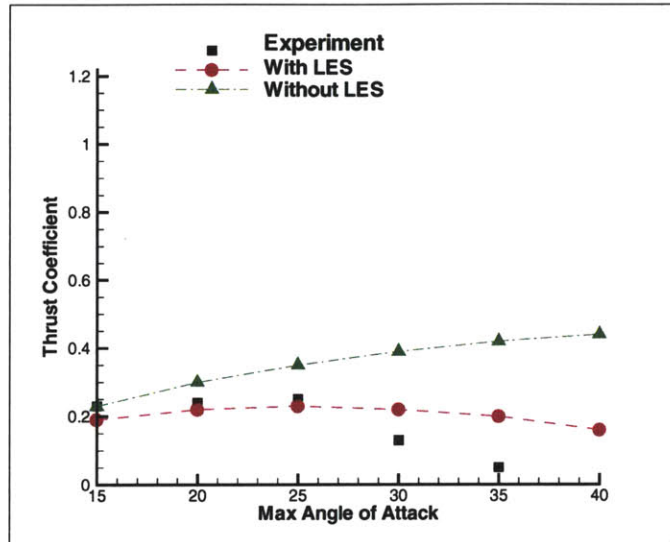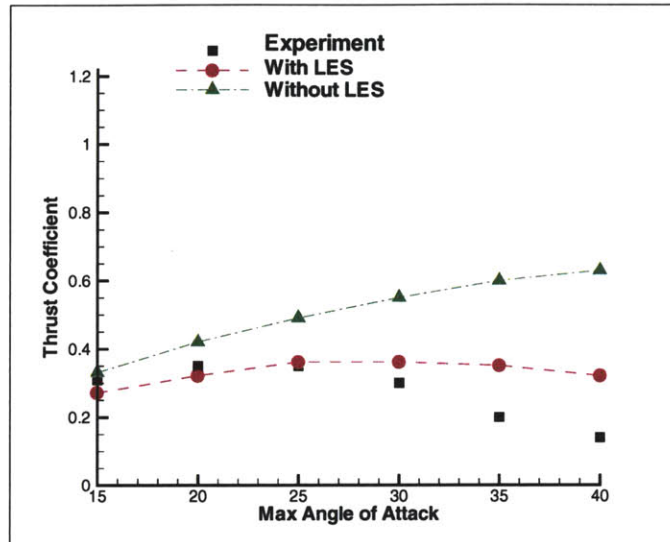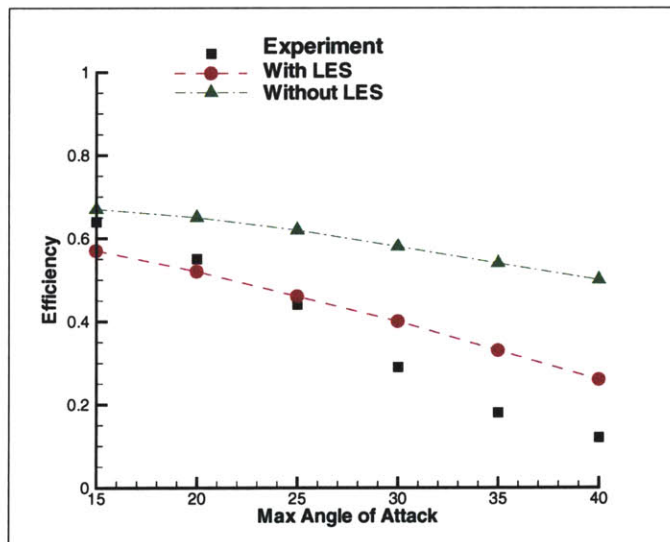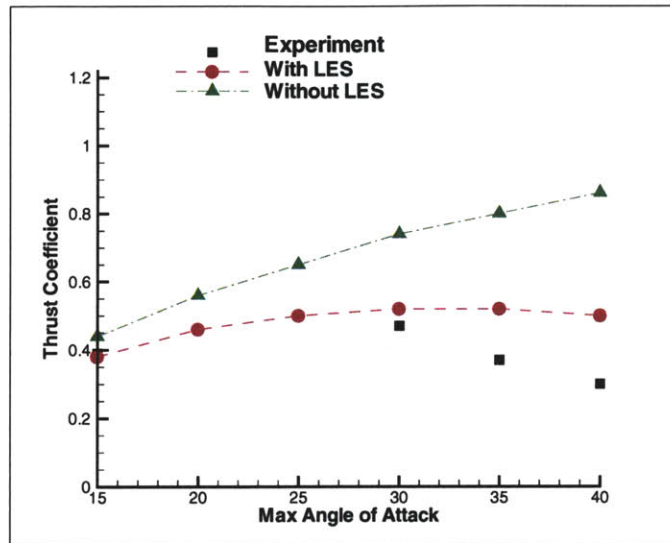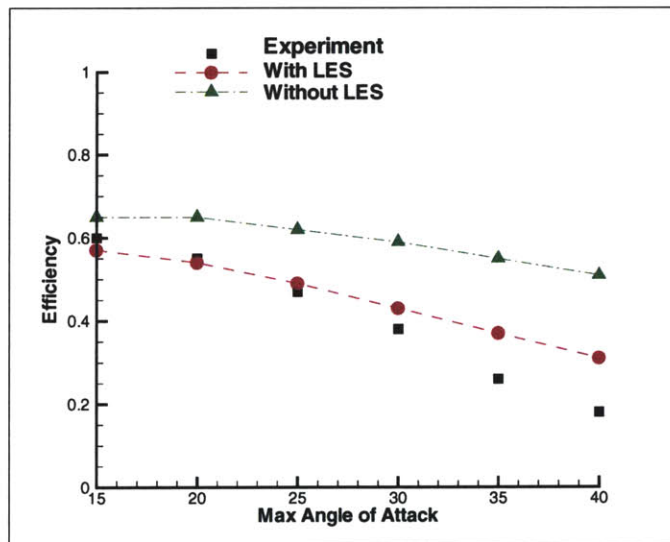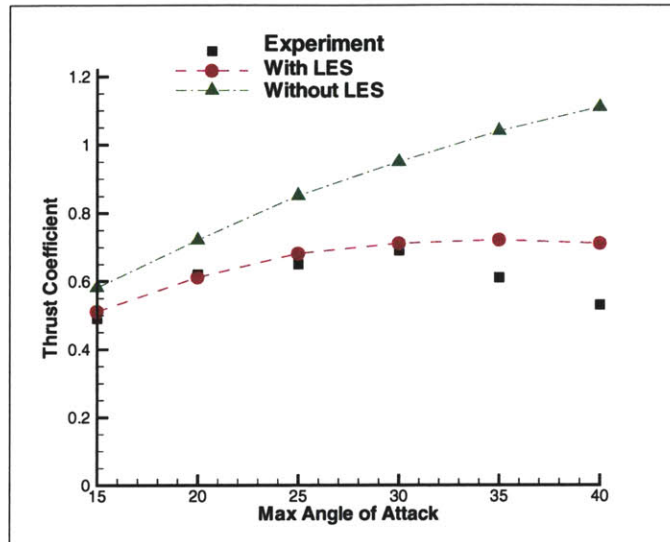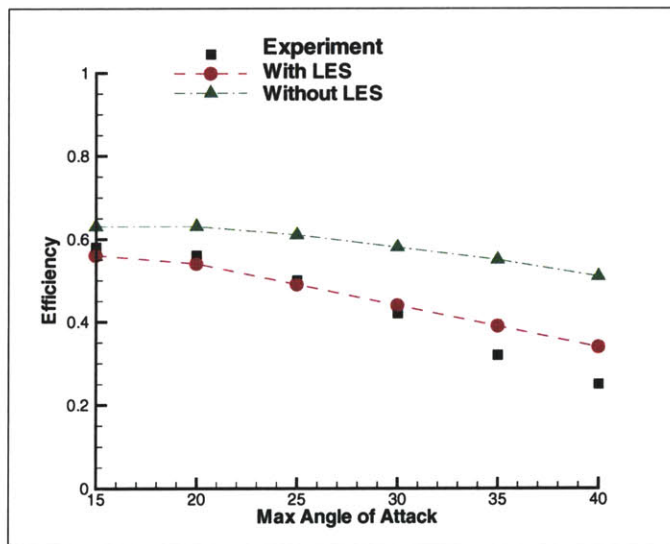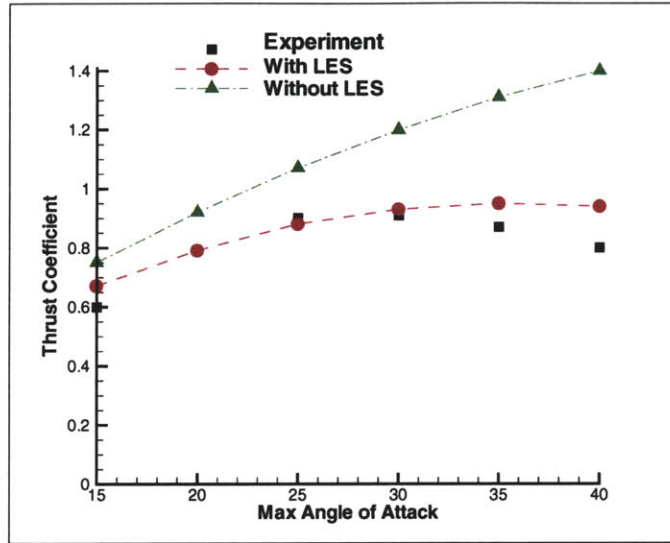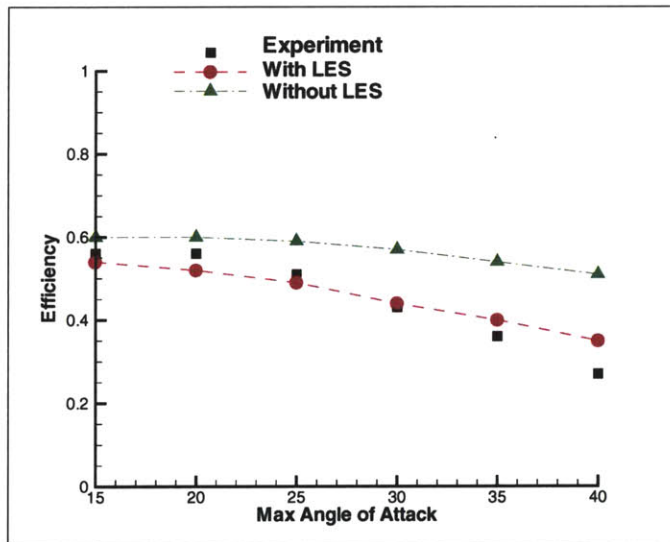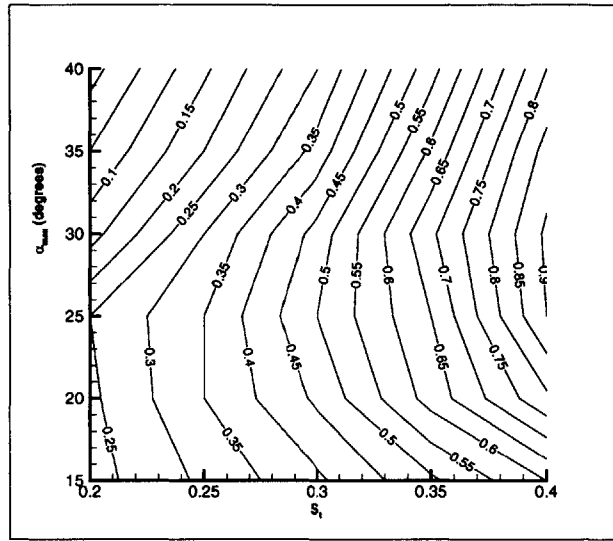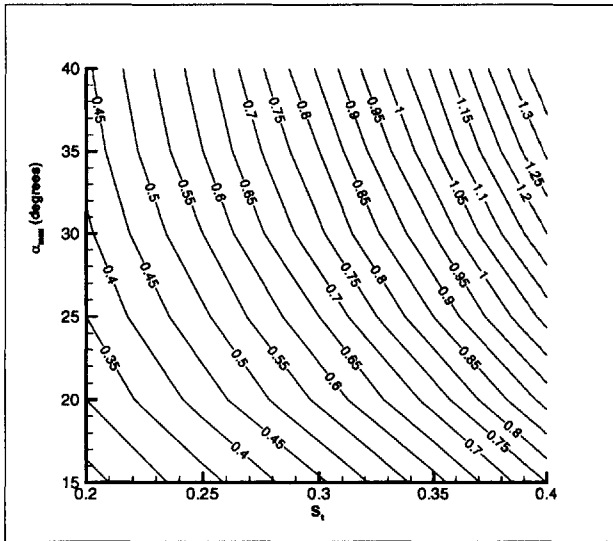
(a) Mean thrust coefficient
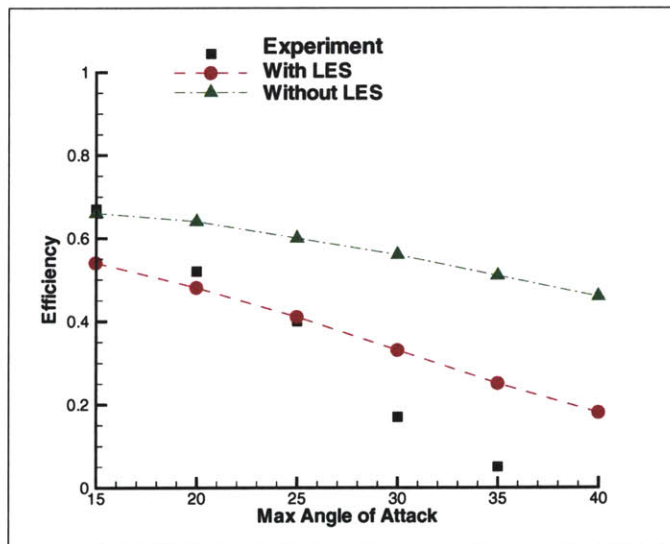
(b) Mean efficiency

Figure 6-10: Strouhal number $S_t = 0.20$.
Mean thrust coefficient and mean efficiency of a heaving-pitching foil with heave chord ratio $h_0/c = 0.75$ and phase angle between heave and pitch $\psi = 90^o$.

(a) Mean thrust coefficient

(b) Mean efficiency

Figure 6-11: Strouhal number $S_t = 0.25$.
Mean thrust coefficient and mean efficiency of a heaving-pitching foil with heave chord ratio $h_0/c = 0.75$ and phase angle between heave and pitch $\psi = 90^o$.
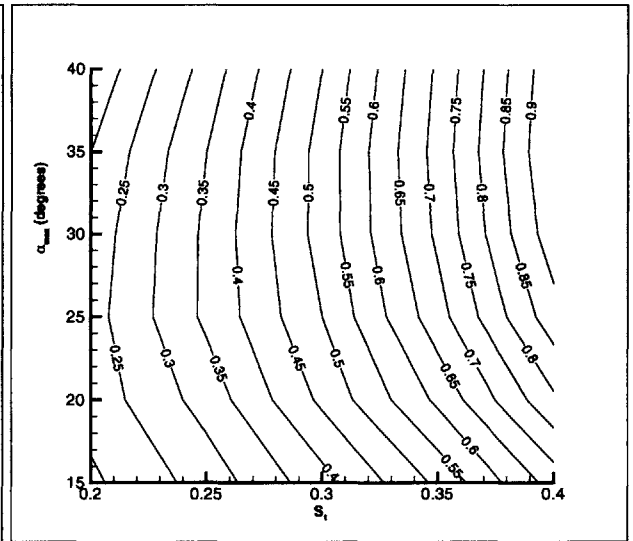
(a) Mean thrust coefficient

(b) Mean efficiency

Figure 6-12: Strouhal number $S_t = 0.30$.
Mean thrust coefficient and mean efficiency of a heaving-pitching foil with heave chord ratio $h_0/c = 0.75$ and phase angle between heave and pitch $\psi = 90^o$.

(a) Mean thrust coefficient

(b) Mean efficiency

Figure 6-13: Strouhal number $S_t = 0.35$.
Mean thrust coefficient and mean efficiency of a heaving-pitching foil with heave chord ratio $h_0/c = 0.75$ and phase angle between heave and pitch $\psi = 90^o$.

(a) Mean thrust coefficient

(b) Mean efficiency

Figure 6-14: Strouhal number $S_t = 0.40$.
Mean thrust coefficient and mean efficiency of a heaving-pitching foil with heave chord ratio $h_0/c = 0.75$ and phase angle between heave and pitch $\psi = 90^o$.

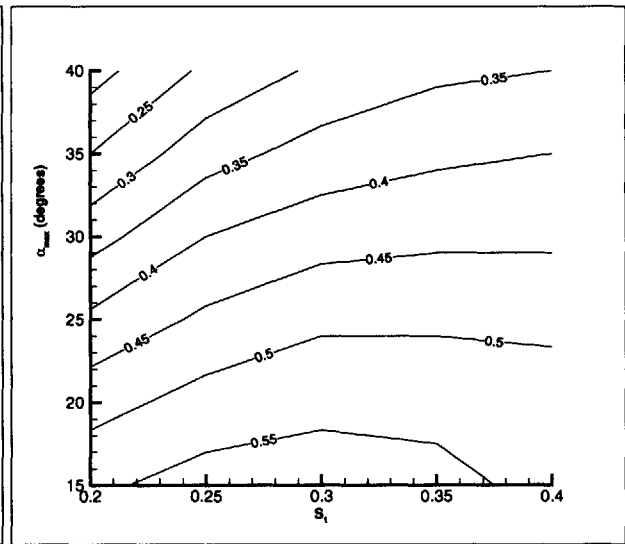(a) Experiments (Read 2000)

(b) Without LES

(c) With LES

Figure 6-15: Contours of the mean thrust coefficient of a heaving-pitching foil with heave chord ratio $h_0/c = 0.75$ and phase angle between heave and pitch $\psi = 90^o$.
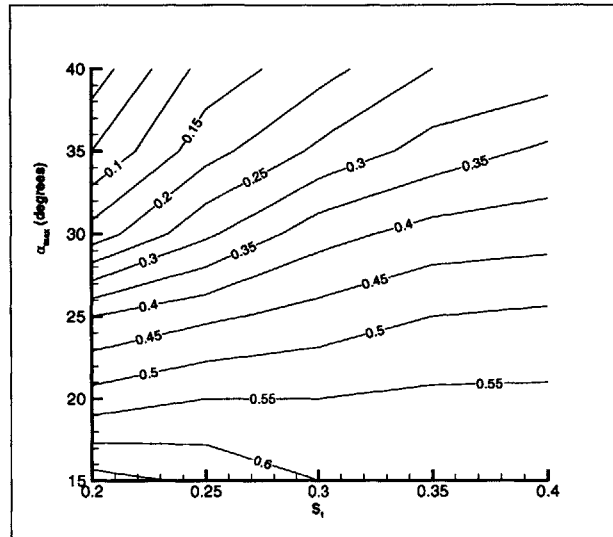
(a) Experiments (Read 2000)
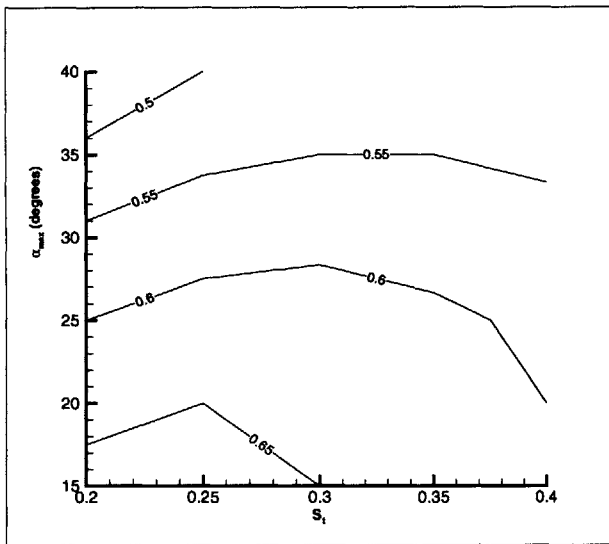
(b) Without LES

(c) With LES

Figure 6-16: Contours of the mean efficiency of a heaving-pitching foil with heave chord ratio $h_0/c = 0.75$ and phase angle between heave and pitch $\psi = 90^o$.

86

separation to happen for the airfoil NACA0012 we use in our simulation. Thus at the maximum angle of attack $\alpha_{max} = 15^o$, the leading-edge separation hardly happens.

It is notable from Figure 6-4 to Figure 6-9 that without the leading-edge separation, the maximum efficiency occurs when S_t is within the range $0.2 \sim 0.3$, which corresponds to the maximum wake amplification (Triantafyllou et al. 1993). However, when the leading-edge separation effect is included, the maximum efficiency is reached at much higher Strouhal numbers.

A possible explanation of this shift of the optimal Strouhal number involves the interaction between the vortices shed from the leading edge and the trailing edge (Zhu private communication 2004). As illustrated experimentally by Gopalkrishnan et al. (1994) and computationally by Zhu et al. (2002), there exist two distinguishable modes when two wake sheets interact with each other. One is called constructive interaction, featuring zero phase difference between the two vortex sheets, which will strengthen each other. It was found that the maximum mean thrust is achieved by employing this mode. The other is destructive interaction, in which the phase difference is close to π so that the vortices tend to diminish each other. Although the destructive mode does not help increase the thrust, it corresponds to the maximum propulsion efficiency.

In our heaving-pitching motion of the foil, the two vortex wake sheets shed from the leading edge and the trailing edge interact with each other. We assume that the leading-edge vortices lag behind the trailing-edge vortices by a phase difference ψ_0. Because the leading-edge vortices must travel downstream for a distance c before interacting with the trailing-edge vortices, the total phase difference between the two vortex sheets is $\psi_0 + 2\pi f c/U$, where f is the frequency of the heaving-pitching motion.

If we consider only the heaving motion, then $\psi_0 = \pi$. To obtain the destructive mode of the two wake sheets, we need $fc/U = 1.0$, which will result in $S_t = 1.5$ and 2.0 for $h_0/c = 0.75$ and 1.0 respectively. To compromise between the optimal efficiency of a single wake and the efficiency enhancement related to the destructive interactions, the optimal Strouhal number is expected to be larger than that for a single wake as we observe from both the experiments and our numerical simulations.

87

6.6.2 Simulation Results for $h_0/c = 1.0$

Additional simulations are carried out for cases with a larger heaving amplitude $h_0/c = 1.0$. From this set of results, we can draw similar conclusions as from the results for $h_0/c = 0.75$.

6.7 Conclusion

The mean thrust coefficient and propulsion efficiency are compared with those from the experiments (Read 2000) extensively for $h_0/c = 0.75$ and $h_0/c = 1.0$ in the parameter range of $S_t \in (0.2, 0.4)$ and $\alpha_{max} \in (15^o, 40^o)$. The inclusion of the leading-edge separation significantly improves the prediction of the mean thrust coefficient and propulsion efficiency, especially at medium maximum angles of attack ($15^o < \alpha_{max} < 30^o$). Although there is still discrepancy between the numerical results and those of the experiments for $\alpha_{max} > 30^o$, the prediction with leading-edge separation is much improved compared with that without leading-edge separation. As the Strouhal number increases, the performance of our simulation with the leading-edge separation becomes better.

Without the leading-edge separation, the maximum efficiency occurs when S_t is within the range $0.2 \sim 0.3$, which corresponds to the maximum wake amplification (Triantafyllou *et al.* 1993). However, when the leading-edge separation effect is included, the maximum efficiency is reached at much higher Strouhal numbers. A possible explanation of this shift of the optimal Strouhal number involves the interaction between the vortices shed from the leading edge and the trailing edge (Zhu private communication 2004).
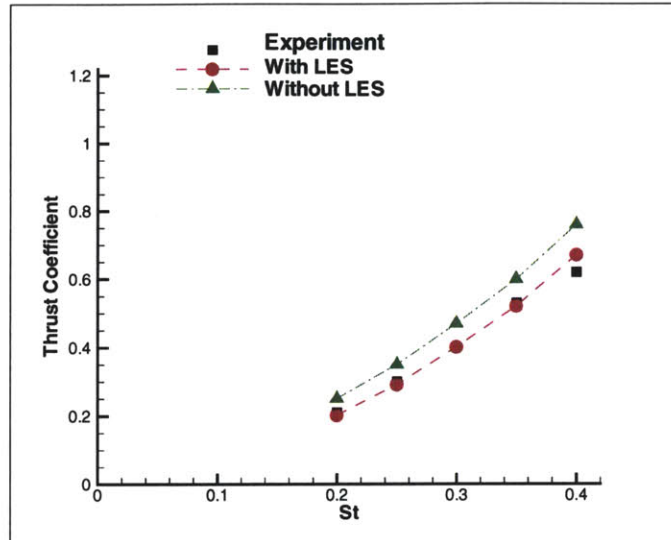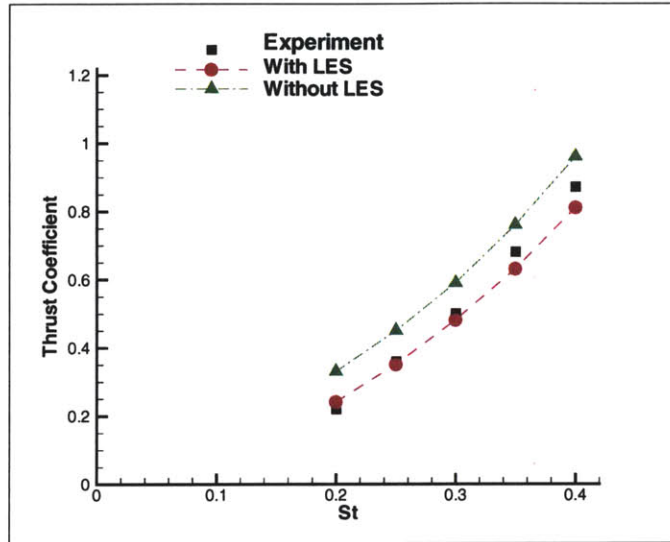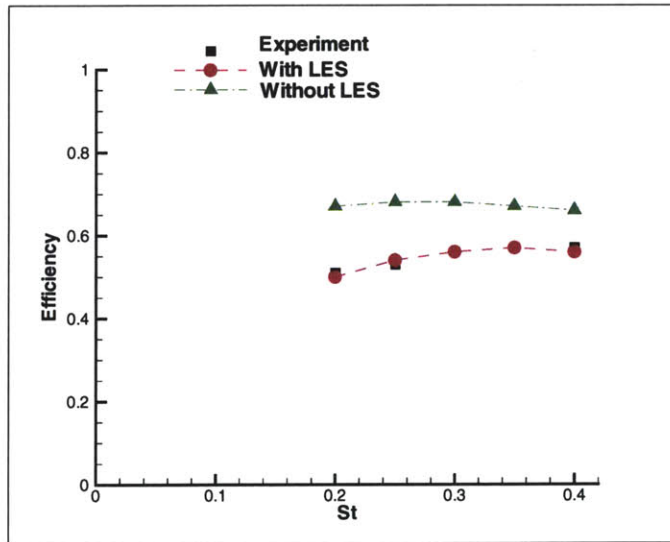
(a) Mean thrust coefficient
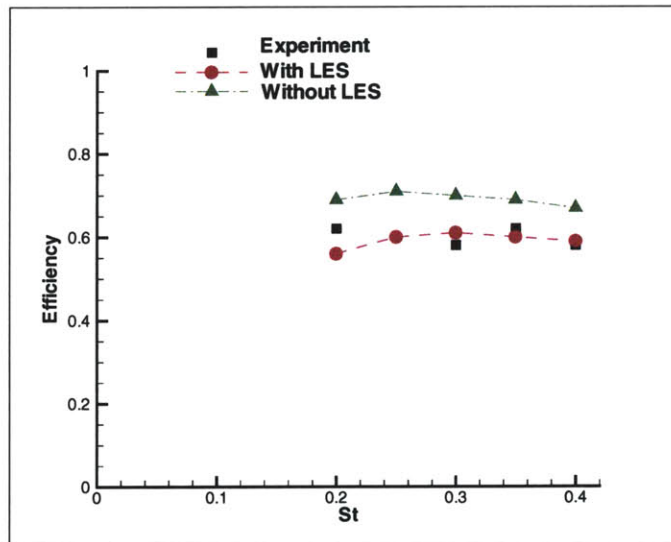
(b) Mean efficiency

Figure 6-17: Maximum angle of attack $\alpha_{max} = 15^o$.
Mean thrust coefficient and mean efficiency of a heaving-pitching foil with heave chord ratio $h_0/c = 1.0$ and phase angle between heave and pitch $\psi = 90^o$.

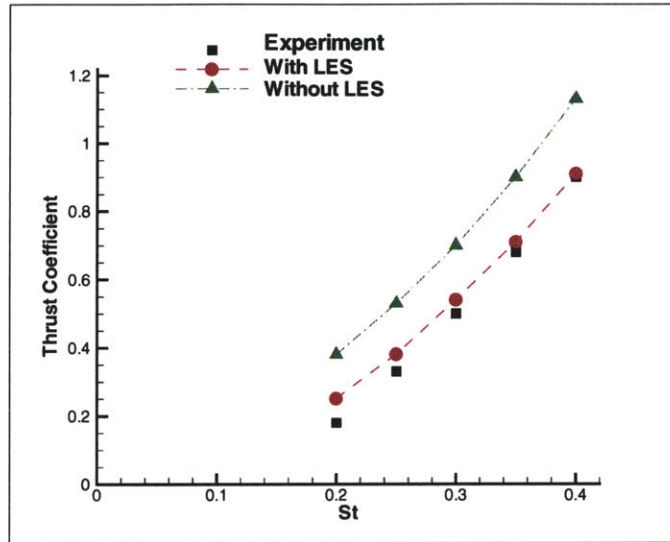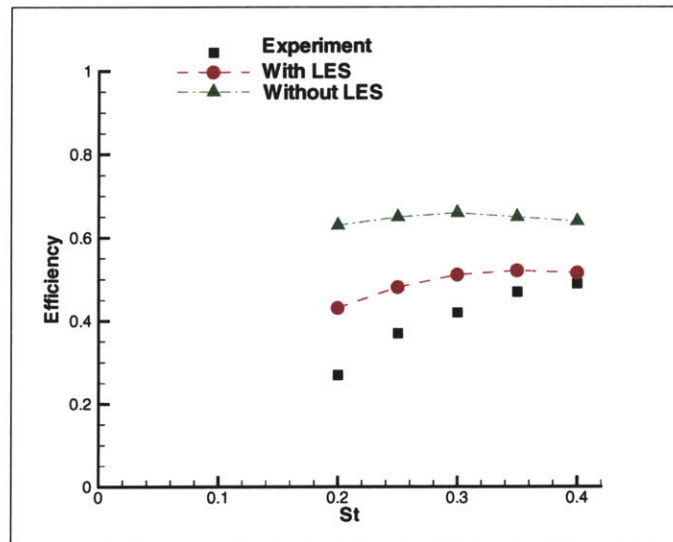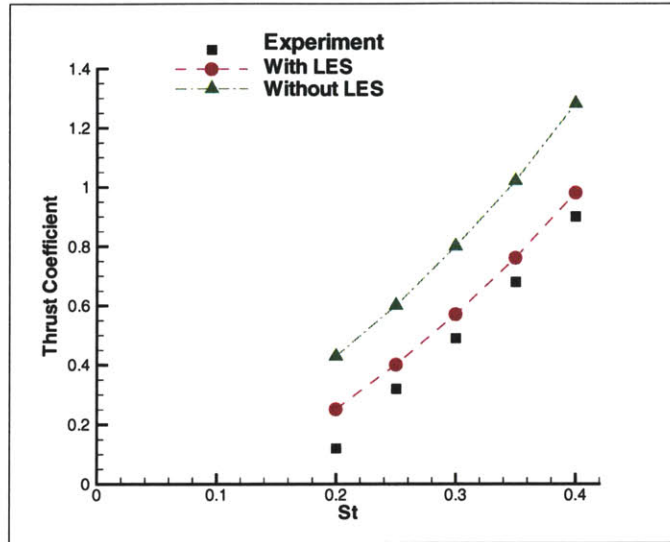(a) Mean thrust coefficient

(b) Mean efficiency

Figure 6-18: Maximum angle of attack $\alpha_{max} = 20^o$.
Mean thrust coefficient and mean efficiency of a heaving-pitching foil with heave chord ratio $h_0/c = 1.0$ and phase angle between heave and pitch $\psi = 90^o$.
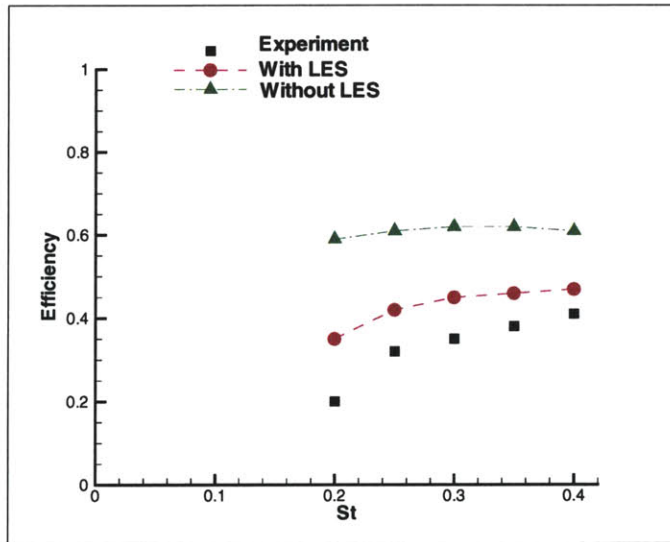
(a) Mean thrust coefficient

(b) Mean efficiency

Figure 6-19: Maximum angle of attack $\alpha_{max} = 25^o$.
Mean thrust coefficient and mean efficiency of a heaving-pitching foil with heave chord
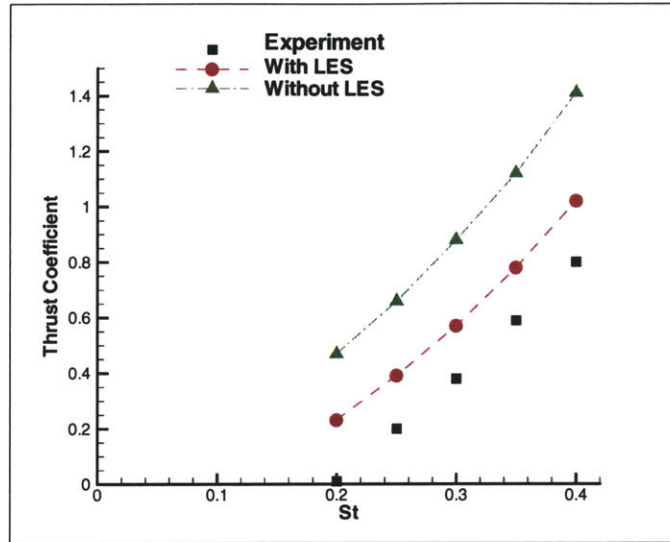ratio $h_0/c = 1.0$ and phase angle between heave and pitch $\psi = 90^o$.
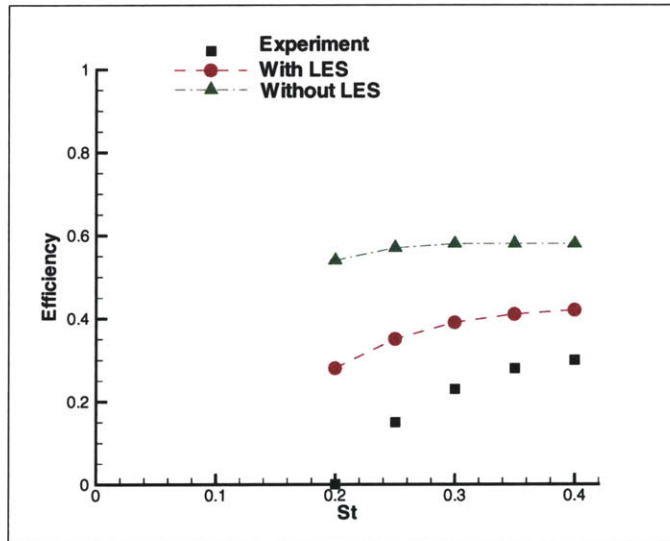
91

(a) Mean thrust coefficient

(b) Mean efficiency

Figure 6-20: Maximum angle of attack $\alpha_{max} = 30^o$.
Mean thrust coefficient and mean efficiency of a heaving-pitching foil with heave chord ratio $h_0/c = 1.0$ and phase angle between heave and pitch $\psi = 90^o$.
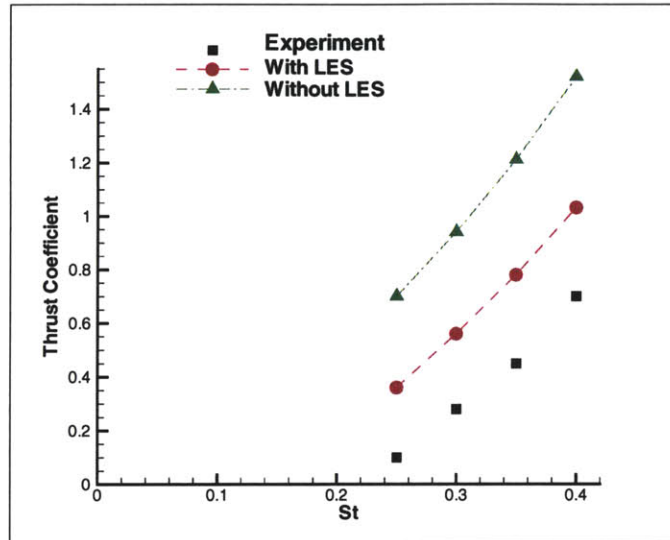
(a) Mean thrust coefficient

(b) Mean efficiency

Figure 6-21: Maximum angle of attack $\alpha_{max} = 35^o$.
Mean thrust coefficient and mean efficiency of a heaving-pitching foil with heave chord ratio $h_0/c = 1.0$ and phase angle between heave and pitch $\psi = 90^o$.

(a) Mean thrust coefficient

(b) Mean efficiency

Figure 6-22: Maximum angle of attack $\alpha_{max} = 40^o$.
Mean thrust coefficient and mean efficiency of a heaving-pitching foil with heave chord ratio $h_0/c = 1.0$ and phase angle between heave and pitch $\psi = 90^o$.
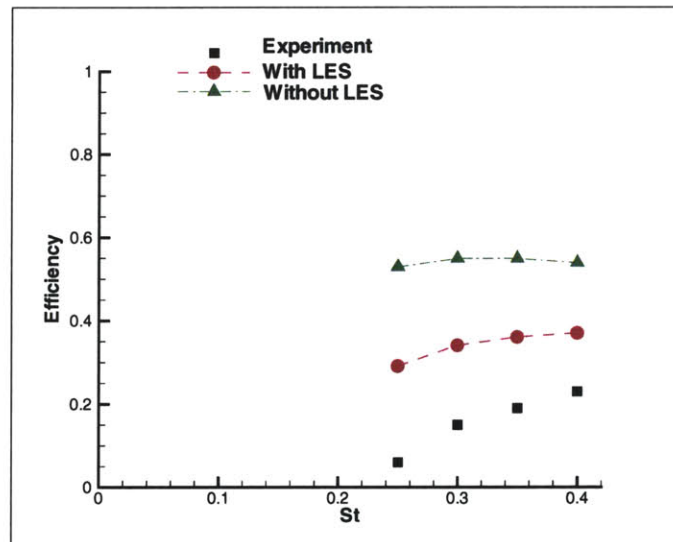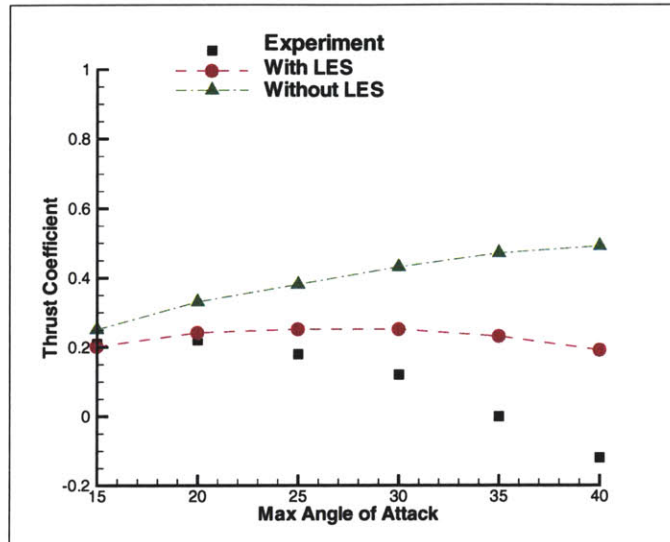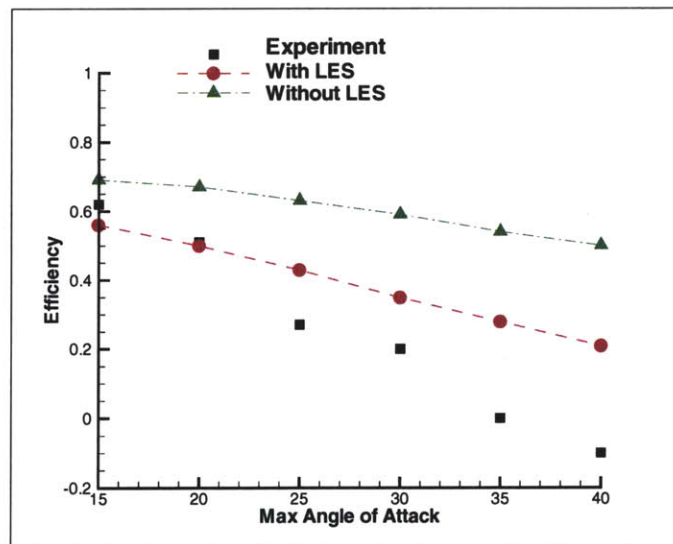
94

(a) Mean thrust coefficient

(b) Mean efficiency

Figure 6-23: Strouhal number $S_t = 0.20$.
Mean thrust coefficient and mean efficiency of a heaving-pitching foil with heave chord ratio $h_0/c = 1.0$ and phase angle between heave and pitch $\psi = 90^o$.

(a) Mean thrust coefficient

(b) Mean efficiency

Figure 6-24: Strouhal number $S_t = 0.25$.
Mean thrust coefficient and mean efficiency of a heaving-pitching foil with heave chord ratio $h_0/c = 1.0$ and phase angle between heave and pitch $\psi = 90^o$.
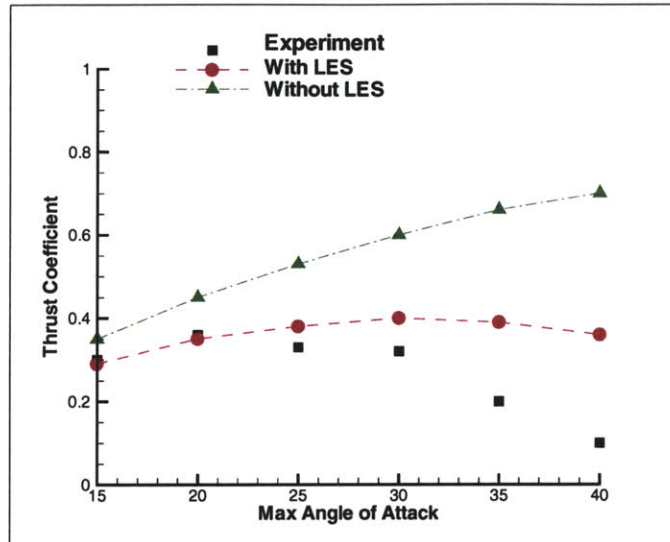
96

(a) Mean thrust coefficient

(b) Mean efficiency

Figure 6-25: Strouhal number $S_t = 0.30$.
Mean thrust coefficient and mean efficiency of a heaving-pitching foil with heave chord ratio $h_0/c = 1.0$ and phase angle between heave and pitch $\psi = 90^o$.
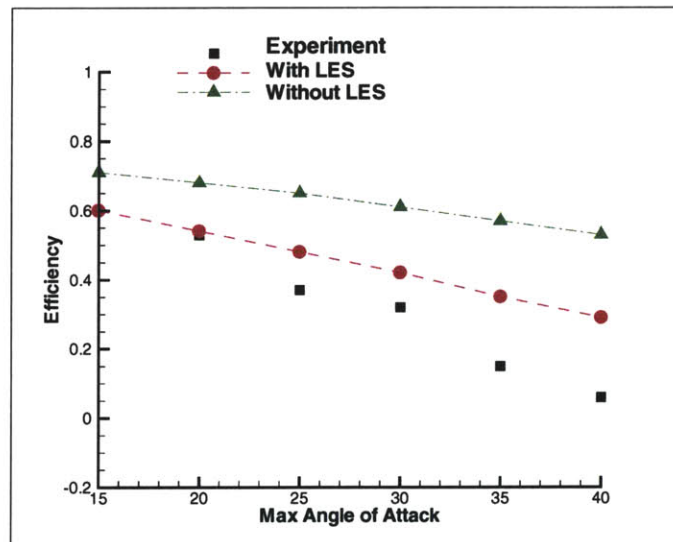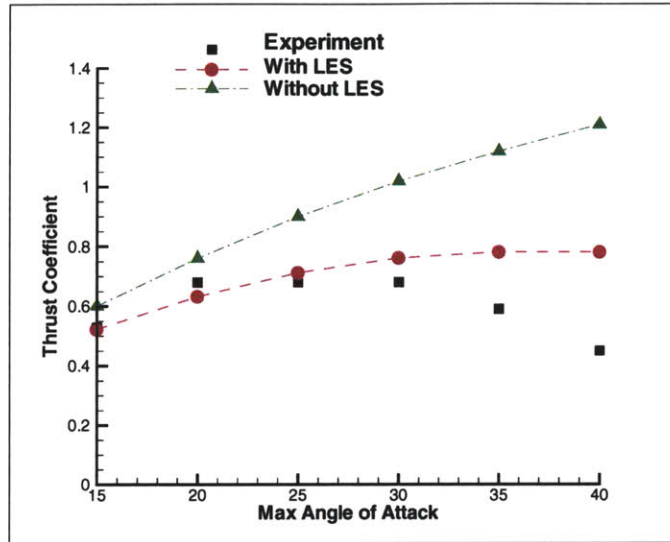
(a) Mean thrust coefficient
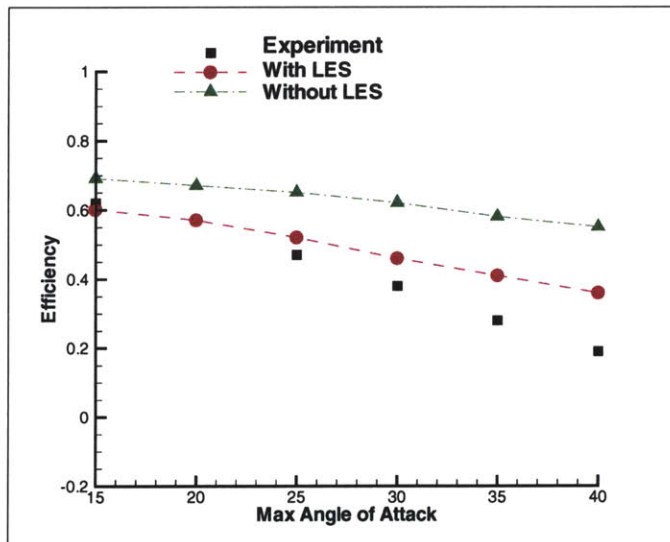
(b) Mean efficiency

Figure 6-26: Strouhal number $S_t = 0.35$.
Mean thrust coefficient and mean efficiency of a heaving-pitching foil with heave chord ratio $h_0/c = 1.0$ and phase angle between heave and pitch $\psi = 90^o$.
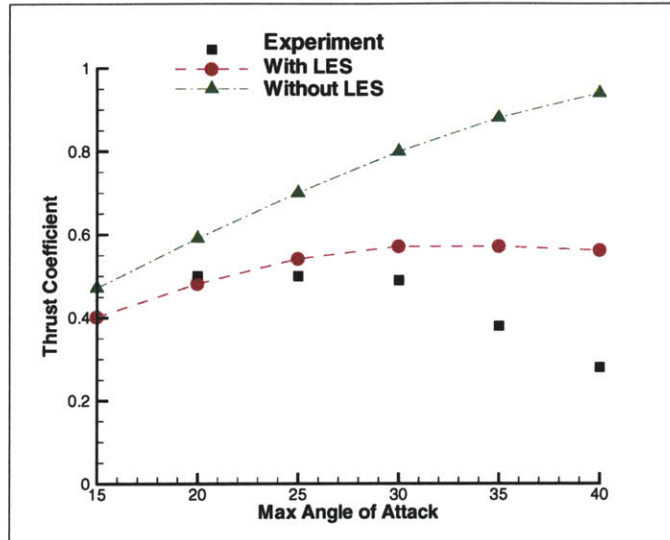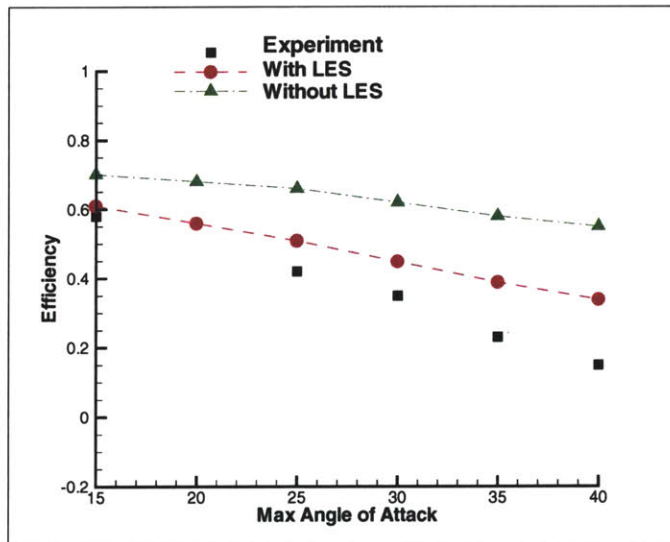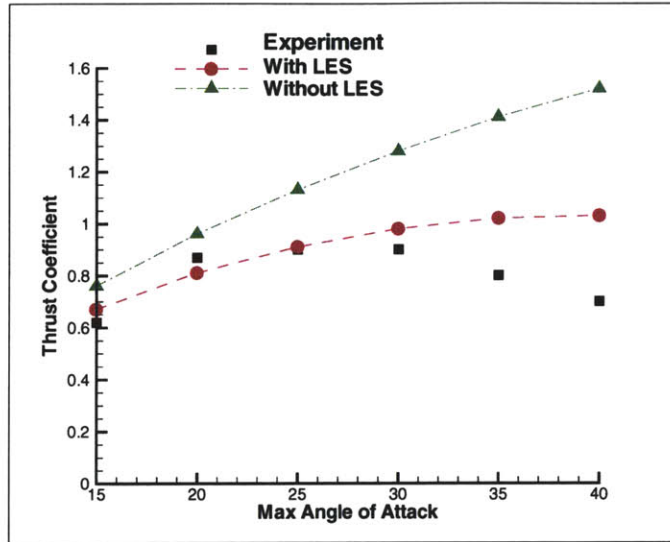
(a) Mean thrust coefficient
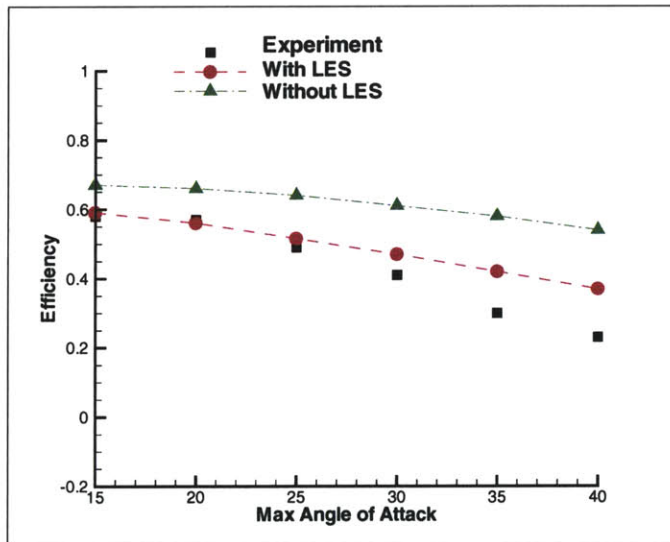
(b) Mean efficiency

Figure 6-27: Strouhal number $S_t = 0.40$.
Mean thrust coefficient and mean efficiency of a heaving-pitching foil with heave chord ratio $h_0/c = 1.0$ and phase angle between heave and pitch $\psi = 90^o$.

(a) Experiments (Read 2000)
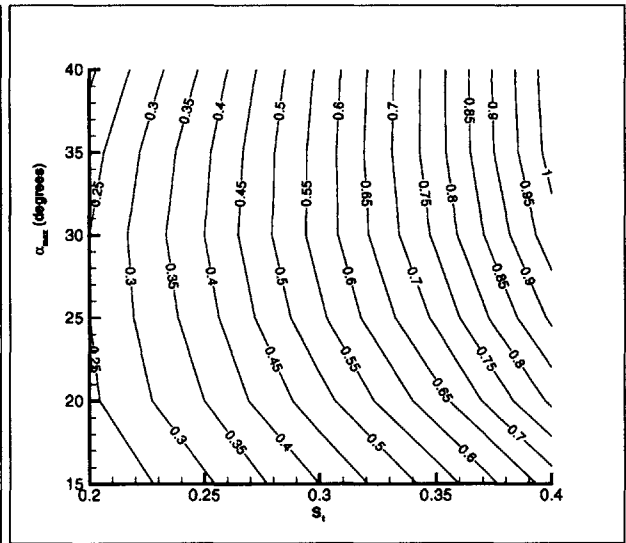
(b) Without LES

(c) With LES

Figure 6-28: Contours of the mean thrust coefficient of a heaving-pitching foil with heave chord ratio $h_0/c = 1.0$ and phase angle between heave and pitch $\psi = 90^o$.
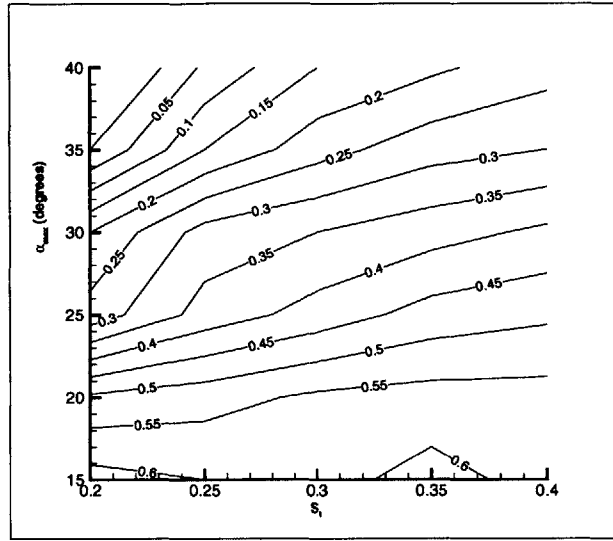
(a) Experiments (Read 2000)
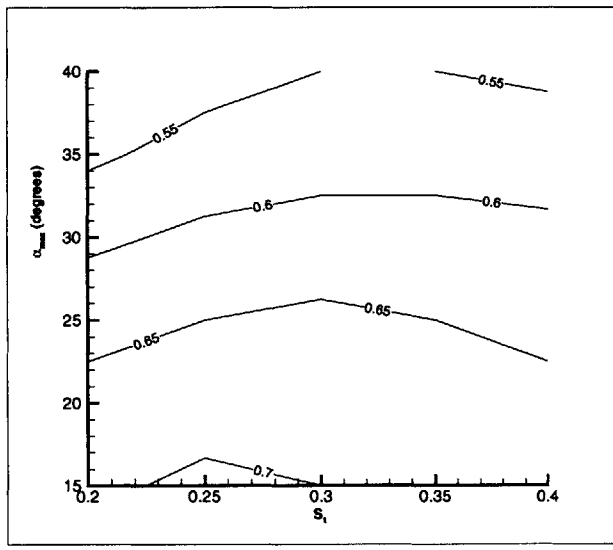
(b) Without LES

(c) With LES

Figure 6-29: Contours of the mean efficiency of a heaving-pitching foil with heave chord ratio $h_0/c = 1.0$ and phase angle between heave and pitch $\psi = 90°$.

101

Chapter 7

Conclusion and Discussion
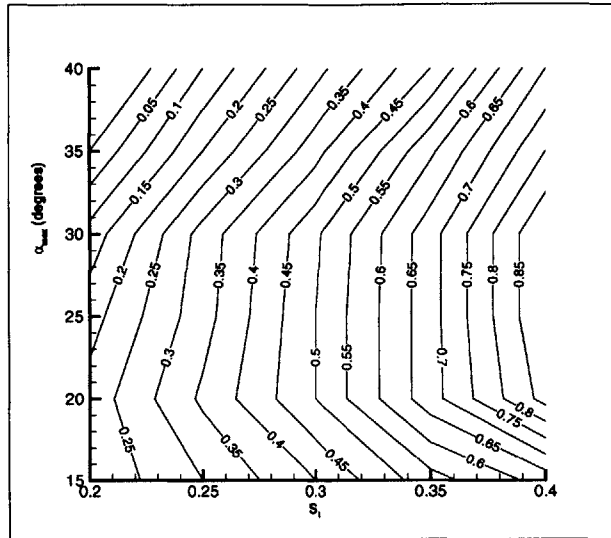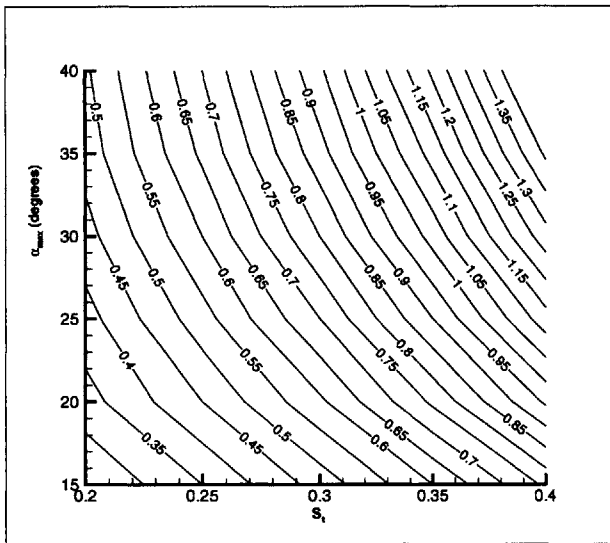
The boundary element simulation of the unsteady fluid dynamics for an oscillating foil is conducted with the potential flow assumption. A leading-edge separation model is included in the simulations to account for the vortices shed near the leading edge. In this model, the leading-edge separation is represented by a thin shear layer similar to the trailing-edge separation. Because of the finite curvature of the leading-edge of the foil, the location for the leading-edge separation is discussed and a separation criterion associated with the adverse pressure gradient is used in the simulation. To resolve the numerical difficulty of the penetration of the wake into the foil body, the pre-check technique is applied in the simulation. Finally the heaving-pitching motions of an oscillating foil are simulated by a low order panel method with an important modification.

In this chapter, the conclusion of our numerical simulation results is summarized and the discussion of further possible improvements of our leading-edge separation model is presented.

7.1 Conclusion

The mean thrust coefficient and propulsion efficiency are compared with those from the experiments (Read 2000) extensively for $h_0/c = 0.75$ and $h_0/c = 1.0$ in the parameter range of $S_t \in (0.2, 0.4)$ and $\alpha_{max} \in (15^o, 40^o)$.

102

The inclusion of the leading-edge separation significantly improves the prediction of the mean thrust coefficient and propulsion efficiency, especially at medium maximum angles of attack ($15^o < S_t < 30^o$). Although there is still discrepancy between the numerical results and those of the experiments for $\alpha_{max} > 30^o$, the prediction with leading-edge separation is much improved compared with that without leading-edge separation. As the Strouhal number increases, the performance of our simulation with the leading-edge separation becomes better.

7.2 Discussion

As the maximum angle of attack further increases increases, the prediction with our leading-edge separation model does not compare well with that of the experiments although it is much better than that without leading-edge separation. The reason may be that when the maximum angle of attack is large, the leading-edge vortices may break down and do not appear like a thin vortex sheet in the near field of the foil as we assume in our modeling.

However, we tried to approximate that by using multiple vortex sheets shed from the leading edge. Instead of one single vortex sheet shed from the leading-edge separation location, a group of the vortex sheets is shed from the leading-edge separation area. However, the resulting forces do not become better when compared with those from the experiments. We consider two vortex sheets shed from the leading-edge, one shed from the separation location we define and the other shed from the location behind the separation location we define.

Figure (7-1) shows the strength of one of the two vortex sheets which is shed from the separation location by our separation criterion and the strength of the other vortex sheet which is shed behind the separation location. We can see that the one shed behind the separation location is much weaker than the one shed ahead of the separation location. The modeling of multiple vortex sheets is not a good candidate to model the complex leading-edge separation when the maximum angle of attack is very high. High maximum angles of attack may cause the vortex breakdown in the
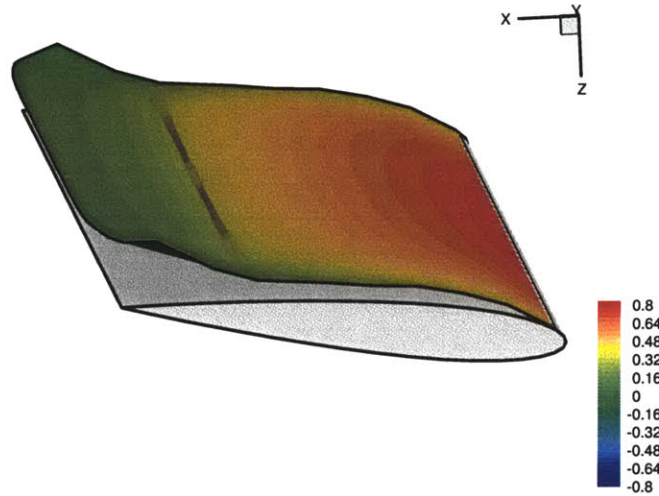
(a) The strength of one of the two leading-edge vortex sheets shed from the separation location we define.
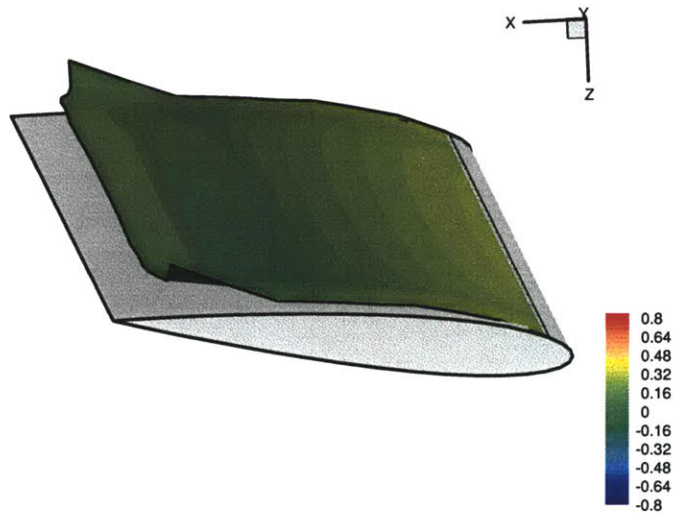
(b) The strength of the other of the two leading-edge vortex sheets behind the separation location we define.

Figure 7-1: The strengths of the two leading-edge vortex sheets. The parameters are: $U = 0.4m/s$, $S_t = 0.30$, $\alpha_{max} = 30^o$, $h_0/c = 0.75$, $\psi = 90^o$.

near field of the foil for the vortex shed from the leading edge. The review about this phenomenon of vortex breakdown can be found in Hall (1972).

Further we may improve our modeling of the separation location by the more complex separation criteria discussed in the review of Smith (1986). In his review, he talked about two-dimensional and three-dimensional, steady and unsteady boundary layer separation and the separation criteria.

One comment about our numerical method is that an alternative Kutta condition in the boundary element method may be used to improve the results of our numerical simulations because accurate determination of the circulations is crucial and the circulations are mainly decided by the Kutta condition (Hess 1990). Therefore, the specification of the Kutta condition is more important than any other aspects of the numerical implementation.

The Kutta condition states that the velocity should leave the sharp trailing edge smoothly and remain finite. According to this statement, in numerical simulation, we should keep the pressure the same on the upper surface of the trailing edge and on the lower surface of the trailing edge. Since the equal pressure condition is nonlinear in the singularities, a linear alternative of the Kutta condition is chosen by most researchers so that the whole problem can be solved linearly. In our simulation, we also use the linear alternative of the Kutta condition. However, this can lead to nonphysical pressure mismatch at the trailing edge (Hess 1990). The details of implementation of the numerical pressure Kutta condition can be found in Hsin (1990). In his simulation of the unsteady propellers, the unsteady pressure Kutta condition is described and the algorithm of implementation is introduced.

Because we modeled the leading-edge separation similar to the trailing-edge separation, we use the Kutta condition also at the leading edge. Thus the pressure mismatch at the leading-edge may have significant effects.

7.3 Future Work

To summarize our discussion above, we recommend the future work here:

- The equal pressure Kutta condition, which may improve the accuracy of our simulation, can be used to replace the linear Kutta condition.

- At high maximum angles of attack, our leading-edge separation model may be un-physical when the leading-edge vortices break down. More physics may be incorporated into the leading-edge separation model at high maximum angles of attack when a single vortex sheet could not model the leading-edge separation well.

- For oscillating foils, optimal thrust can be achieved when the Strouhal number is in the range between 0.25 and 0.35 (Triantafyllou *et al.* 1991). Triantafyllou *et al.* (1995) found that efficiency was at its peak when the maximum angle of attack was between 15° and 25° for oscillating foil. In the parameter range of $S_t \in (0.25, 0.35)$ and $\alpha_{max} \in (15^o, 25^o)$, our leading-edge model performs remarkably well. We can actually do a parameter optimization to achieve the desired thrust or efficiency.

References:

Anderson J.M. 1996 Vorticity control for efficient propulsion. Doctoral thesis, Massachussetts Institute of Technology and the Woods Hole Oceanographic Institution.

Anderson J.M., Streitlien K., Barret D.S. and Triantafyllou M.S. 1998 Oscillating foils for high propulsion efficiency. J. Fluid Mech., 360:41-72

Barker S.J. and Crow S.C. 1977 The motion of two-dimensional vortex pairs in a ground effect. J. Fluid Mech., 82:659-671.

Campbell M. Concept development of an oscillating tidal power generator. Proceedings of ASME Fluids Engineering Division Summer Meeting, Montreal, July 2002.

Chen S.H. and Williams M.H. 1987 A panel method for counter rotating propfans. AIAA-1987-1890.

Curle H. 1967 A Two Parameter method for Calculating the Two-Dimensional Incompressible Laminar Boundary Layer. J.R. Aero Soc., 71

Doligalski T.L., Smith C.R. and Walker J.D.A. 1994 Vortex interactions with walls. Annu. Rev. Fluid. Mech., 26:573-616.

Drucker E.G. and Lauder G. V. 2002 Experimental hydrodynamics of fish locomotion: functional insights from wake visualization. Integ. and Comp. Biol., 42:243-257.

Gopalkrishnan R., Triantafyllou M., Triantafyllou G. and Barrett D. 1994 Active vorticity control in a shear flow using a flapping foil. J. Fluid Mech., 274:1-21.

Hall M.G. 1972 Vortex breakdown. Annu. Rev. Fluid. Mech., 4: 195-218

Hess J.L. 1990 Panel methods in computational fluid dynamics. Annu. Rev. Fluid. Mech., 22:255-274.

Hsin C.-Y. 1990 Development and analysis of panel methods for propellers in unsteady flow. MIT PhD thesis.

Katz J. 1981 A discrete vortex method for the non-steady separated flow over an airfoil. J. Fluid Mech., 102:315-328.

Katz J. and Plotkin A. 1991 Low-speed Aerodynamics: from Wing Theory to Panel Methods., McGraw-Hill.

Koochesfahani M.M. 1989 Vortical patterns in the wake of an oscillating airfoil. AIAA J., 27:1200-1205.

Letcher J.S. 1989 Convergence of lift and drag predictions by a Morino panel method (VSAERO). AIAA J., 27:1019-1020.

Lewin G.C. and Haj-hariri H. 2003 Modelling thrust generation of a two-dimensional heaving airfoil in a viscous flow. J. Fluid Mech., 492:339-362.

Liu H., Ellington C.P., Kawachi K., Berg C. and Willmott A.P. 1998 A computational fluid dynamics study of hawkmoth hoving. J. Exp. Biol., 201:461-477.

Liu H. and Kawachi K. 1998 A numerical study of insect flight. J. Comput. Phys., 146:124-156.

Maresca C. Favier D. and Rebont J. 1979 Experiments on an aerofoil at high angle of incidence in longitudinal oscillations. J. Fluid Mech., 92:671-690

Minotti F. O. 2002 Unsteady two-dimensional theory of a flapping wing. Phys. Rev. E, 66. 051907.

Moore F.K. 1958 On the separation of the unsteady laminar boundary layer. Boundary-Layer Research. ed. H.G. Görtler. Springer. 296-310.

Ohmi K., Coutaneau M., Loc T.P. and Dulleu A. 1990 Vortex formation around an oscillating and translating airfoil at large incidences. J. Fluid Mech., 211:37-60.

Ohmi K., Coutaneau M., Daube O. and Loc T.P. 1991, Further experiments on vortex formation around an oscillating and translating airfoil at large incidences. J. Fluid Mech., 225: 607-630.

Peace A.J. and Riley N. 1983 A viscous vortex pair in ground effect. J. Fluid Mech., 129:409-426.

Polidoro V. 2003 Flapping foil propulsion for cruising and hovering autonomous underwater vehicles. Master Thesis, Massachussetts Institute of Technology.

Prempraneerach P., Hover F.S. and Triantafyllou M.S. 2003 The effect of chordwise flexibility in the thrust and efficiency of a flapping foil. The 13th international symposium on UnmannedUntethered Submersible Technology, Durham, NH.

Rammamurti R. and Sandberg W.C. 2002 A three-dimensional computational study of the aerodynamic mechanisms of insect flight. J. Exp. Biol., 205:1507-1518.

Read D.A. 2001 Oscillating foils for propulsion and maneuvering of ships and underwater vehicles. Master thesis, Massachusetts Institute of Technology.

Rott N. 1956 Unsteady viscous flow in the vicinity of a stagnation point. Q. Appl. Math. 13:444-451.

Sears W. R. and Telionis D.P. 1975 Boundary-layer separation in unsteady flow. SIAM J. Appl. Math. 28:215-235.

Smith F.T. 1986 Steady and unsteady boundary-layer separation. Annu. Rev. Fluid. Mech., 18:197-220.

Taneda S. 1977 Visual study of unsteady separated flows around bodies. Prog. Aerospace Sci. Vol. 17, 287-348.

Taylor G.K., Nudds R.L. and Thomas L.R. 2003 Flying and swimming animals cruise at a Strouhal number tuned for high power efficiency. Nature, 425:707 - 711.

Terzi A. and Chiu T.W. 1997 Modern panel method techniques for modeling wake body interference. AIAA-1997-1829.

Theodorsen T. 1935 General theory of aerodynamic instability and mechanism of flutter. Report No. 496, National Advisory Committee for Aeronautics.

Triantafyllou M.S., Triantafyllou G.S. and Gopalkrishnan R. 1991 Wake mechanics for thrust generation in oscillating foils. Phys. Fluids A, 3:2835-2837.

Triantafyllou G.S., Triantafyllou M.S. and Grosenbaugh M.A. 1993 Optimal thrust development in oscillating foils with application to fish propulsion. J. Fluids Struct., 7:205-224.

Triantafyllou M.S. and Triantafyllou G.S. 1995 An efficient swimming machine. Scientific American, 272:64-70.

Triantafyllou M.S., Triantafyllou G.S. and Yue D.K.P. 2000 Hydrodynamics of fishlike swimming. Annu. Rev. Fluid Mech. 32:33-53

Tuck E.O. 1991 A criterion for leading-edge separation. J. Fluid Mech., 222:33-37.

Wang Z.J. 2000 Vortex shedding and frequency selection in flapping flight. J. Fluid Mech., 410:323-341.

Weymouth D. G., Wilson V. R. and Stern F. 2005 RANS computational fluid dynamics predictions of pitch and heave ship motions in head seas. J. Ship Research,

Vol. 49 2:80-97.

Williams J.C. 1977 Incompressible boundary-layer separation. Annu. Rev. Fluid. Mech., 9:113-144.

Yao Z.X. and Liu D.D. 1998 Vortex Dynamics of blade-blade interaction. Vol. 36, No. 4 AIAA Journal.

Zhu Q., Wolfgang M.J., Yue D.K.P. and Triantafyllou M. S. 2002 Three-dimensional flow structures and vorticity control in fish-like swimming. J. Fluid Mech., 468:1-28.